AN INVESTIGATION INTO THE FABRICATION OF A NEW MINI GAS SENSOR FOR MEDICAL DIAGNOSTIC APPLICATIONS

KATIE JAYNE VAUGHAN

A thesis submitted in partial fulfilment of the requirements of the University of the West of England Bristol, for the degree of Master of Philosophy

This research was carried out in collaboration with Bristol Urological Institute

Department of Applied Science, University of the West of England

AUGUST 2013

Abbreviations

VOC – Volatile organic compound

FDA – Food and Drug Administration

BCC – Business Communications Company

BUI – Bristol Urological Institute

TCR – Temperature coefficient of resistance

UV – Ultra violet

CAD- Computer aided design

CAM-Computer aided manufacture

TWI – The Welding Institute

LGDW - Laser guided direct-write

FGDW – Flow guided direct-write

LIFT – Laser induced forward transfer

C. diff. – Clostridium difficile

GC – Gas chromatography

MS – Mass spectrometry

GCMS – Gas chromatography mass spectrometry

TB – Tuberculosis

OMA – Osmotech Microbial Analyser

ANN – Artificial neural network

Au - Gold

Pt- Platinum

ESL – Electro Science Limited

ESEM- Environmental scanning electron microscope

EDX – Energy dispersive x-ray

ppm – Parts per million

UWE – University of the West of England

UTI – Urinary tract infection

MSP – Micro-spectrophotometer

S.D.– Standard deviation

$R_{0°C}$ – Resistance at 0°C

$R_{100°C}$ – Resistance at 100°C

cfus/ml – Colony forming units/ml

UC - Ulcerative colitis

Acknowledgements

I would like to thank my two supervisors, Professor Norman Ratcliffe and Dr Ben de Lacy Costello for all the help and support they have given me throughout my time at UWE. I would also like to thank Dr Peter Walters at the Centre for Fine Print Research for his kindness and CAD expertise that made creating the files for the sensor designs possible. Thanks also to Dr David Patton for his guidance using the ESEM and for producing the electron micrographs showing metal oxide paste deposited onto the sensor substrates. I am also grateful to all the people working in 2G5, Dr Natasha Mcguire, Dr Steve Smith, Simon Stevens etc for their company and good humour at times when I have needed it most.

Those also due thanks for their technical expertise and support are Dr Helen Goddin from The Welding Institute for the resistance welding of work she conducted on the sensors, Mr John Whitmarsh from ESL for the screen printing work carried out under his supervision, Dr Richard Ewen for his assistance on the electronic/software aspects of the project, Jonathan Williams and Richard Thomson for their assistance in microbiological aspects of the project and Mr Kevin Slater from Manor Farm Engineering for building a manual screen printing bed used in the deposition trials of the metal oxide paste.

I also would like to thank the Bristol Urological Institute, Dr Marcus Drake, the University of the West of England, and grants from the NBHT and the Wellcome Trust for supporting this project.

Finally, I would like to thank my family for supporting me always.

Abstract

This research was part of a larger Wellcome Trust funded project that aimed to create a non-invasive volatile diagnostic device for medical applications, particularly for the detection of *Clostridium difficile* (*C. Diff*) in human stool. The device (OdoReader) consists of a gas chromatography column to separate gaseous mixtures, a metal oxide sensor to detect and respond to individual analytes and an artificial neural network trained to recognise patterns indicative of positive and negative results.

The aim of this MPhil research project was to fabricate the metal oxide gas sensor to work within this device and to conduct a pilot study to assess the potential for using OdoReader to detect urinary tract infections human urine. Sensors that were compatible with existing electronic components were not commercially available, making it essential to fabricate sensors in-house. A preliminary investigation into sensor fabrication techniques was conducted in order to assess the most simple and cost-effective process to fabricate the new sensor. Screen printing was selected and used to deposit conductive pastes onto alumina substrates to produce interdigitated electrodes and a heater element. Three sensor designs were subsequently produced, two designed to be housed in edge connectors (type A), and the third to be mounted onto a transistor can (type B). Initial tests showed that type A sensors would not withstand the operating temperature required (450˚C). Type B sensors required an extra process to join metal wires from the sensor substrate to the transistor can. This process consistently created strong mechanical connections that enabled the sensor to achieve and

maintain the required operation temperature. For this reason this sensor and transistor can combination was selected.

In order to give the sensor substrate its sensing properties, the deposition method of a metal oxide paste (to be applied over the interdigitated electrodes of the sensor substrate) was investigated. An even layer of the metal oxide paste was of extreme importance for this type of sensor and for this reason screen printing was one of the methods considered. For these trials, a custom built screen printing jig (for manual operation) was designed and fabricated. These trials proved unsuccessful for our purposes therefore a doctor blading technique was adopted. After some development this method satisfied the requirements for the sensor and has been used to coat over 50 sensor substrates.

The mean electrical resistance (for 25 sensors) of the metal oxide coating was 116000Ω, S.D.38042Ω. The mean resistance of the heater element (for 26 sensors) was calculated at 10.8Ω at 0°C, S.D. 0.23Ω.

The sensors met OdoReader sensitivity specifications for ≥150% to ethanol (50ppm) with a mean sensitivity (for 25 sensors) of 216% and a S.D. 46%.

As this sensor was designed for medical diagnostic applications, a pilot study was conducted to assess the potential for the detection of bacteria in human urine and the identification of the urinary tract infection (UTI) causing bacteria through volatile organic compound (VOC) analysis. The sensor developed here was used in combination with a gas chromatography (GC) column (OdoReader) to assess urine inoculated with known bacteria.

Five of the most common UTI causing bacteria were used to inoculate the stock urine and left to grow, with samples taken at hourly intervals for VOC analysis. The bacteria chosen for this study were; *K. pneumoniae, S. saprophyticus*, *P. aeruginosa,* E. faecalis *and P. mirabilis*. VOC analysis was undertaken using infected urine that had not been chemically treated and also infected urine treated with a sodium hydroxide solution. Using OdoReader the detection of bacteria in human urine (at UTI levels) was possible by looking at the retention times and percentage responses of significant peaks. It was also found that there is the potential to differentiate between bacteria by looking for the presence of peaks at certain retention time ranges**.**

Table of Contents

Chapter 1 –Gas sensors and fabrication techniques

1.1 General introduction to the utility of gas sensors

There is a growing market for reliable low cost gas sensors. Business Communications Company (BCC) has estimated the global market for gas flow meters, sensors and monitors to be *ca*. $3.9 billion in 2010 and they have predicted the market should approach $5.2 billion by 2015 [1]. The first commercially successful gas sensor was fabricated by Taguchi in 1968 [2]. This sensor used a heated metal oxide based device to detect propane leaks and its successful exploitation significantly reduced the loss of life due to gas explosions. Since then the automobile industry has adopted metal oxide sensor technology for engine management systems. Metal oxide sensors have also been used in "electronic nose" systems (an instrument used for the detection and estimation of gases/vapours or odours) [3]. Due to the robustness, low fabrication costs and high sensitivity of metal oxide sensors, they are of particular interest for our research in trace volatile analysis for disease diagnoses.

1.2 Electronic noses and neural networks applied to gas sensors

An electronic nose is an instrument comprised of three parts: (a) a sampling system, (b) an array of chemical gas sensors producing an array of signals when confronted with a gas, vapour, or odour, and (c) an appropriate pattern-classification system [4].

The first report of a sensor array was presented in the early 1980's by Persaud and Dodd from the University of Warwick [5].

They managed to demonstrate that an array of non-selective sensors could be used to discriminate between simple odours through pattern recognition software. Since then, considerable research into the detection of gases in a number of fields has been carried out. These fields include environmental monitoring, food and drink analysis, medical appliances, and industrial control systems.

Several commercial enterprises have been established since that time and they include Alpha Mos who specialise in the development of electronic nose instruments that use a variety of technologies for odour detection. Osmotech (formally Aromascan) have worked in developing electronic nose technology for the detection of microorganisms as well as critical care diagnostics. Owlstone have created a small (ca.1cm diameter) detection device that can be programmed to detect a wide range of chemical agents in small quantities.

Using electronics to measure and quantify specific odours is desirable, as the draw backs associated with alternative methods such as panels reliant on human olfaction can be eliminated. These drawbacks include unreliable results due to fatigue and individual variability [6].

Artificial neural networks are often used for pattern recognition in electronic nose systems. Inspiration for neural networks originally came from studying information processing mechanisms in biological nervous systems, particularly the human brain. An artificial neural network (ANN) is a mathematical/computational model that transforms a set of input variables into a set of output variables. This transformation is governed by a set of parameters called weights, whose values are set up based on a series of examples. This stage is often referred to

as the learning/training stage. [7] The most important feature of neural networks is their ability to learn a general solution from a set of examples.

1.3 Medical diagnostics through volatile analysis

Medical diagnostics through analysis of volatiles is an emerging area of research. At present there are 6 FDA (Federal Drug Administration) approved medical tests using volatile analyses (see table 1). There are many promising research areas that have been/are being explored. Some examples are:

Diagnosis of *C. diff.* infection by analysing the volatiles from stool using gas chromatography mass spectrometry (GC/MS) [8].

Diagnosis of tuberculosis (TB) by analysing volatiles in breath using electronic nose technology [9].

Diagnosis of ulcerative colitis (UC) by analysing volatiles from stool [10].

Diagnosis of urinary tract infection by analysing volatiles in urine using electronic nose technology [11].

Diagnosis of lung disease by analysing volatiles in breath using mass spectrometry (MS) techniques [12].

Assessing oral malodour using a sulphide sensor (e.g. hydrogen sulphide and methanethiol) [13].

Diagnosis of skin cancer, bladder cancer and breast cancer using trained canines [14,15,16].

Table 1- FDA approved medical tests for volatile analysis

Volatile	Medical condition
Nitric oxide– Increase in breath concentration	Asthma attack
Carbon 13 carbon dioxide increase in breath concentration– Patient eats carbon 13 urea and the bacteria produces carbon 13 carbon dioxide.	*H.pylori* infection
Carbon monoxide – Increase in breath concentration	Jaundice in babies through the increase of bilirubin production and carbon monoxide
Pentane/hydrocarbons – increase in breath concentration.	Heart transplant rejection
Hydrogen	For diagnosing bacterial overgrowth and malabsorption e.g. of fructose
Volatile organic compounds – from urine	Urinary Tract Infections (UTIs)

1.4 OdoReader – a volatile diagnostic device

OdoReader is a volatile diagnostic device that uses a metal oxide sensor in combination with a GC column. OdoReader differs from electronic nose systems in that only a single metal oxide sensor is used to detect volatiles, compared to an array of different sensors used in electronic nose systems. Capillary columns are commonly used in GC analysis and these can either have single or multiple capillaries. The internal walls (a few tenths of a millimetre in diameter) are often coated with a liquid stationary phase i.e. a polymer that interacts with the individual components (analytes) in the gaseous mixture. The speed at which each analyte exits the column (elutes) depends on the way it interacts with the liquid stationary phase inside the column [17].

Figure 1 shows a typical GC set up involving a carrier gas (the mobile phase) that carries the vaporised sample through the column, a heated injection port to introduce and vaporises the sample, a GC column to separate the mixture into individual analytes, a detector that responds to each analyte and a recorder that measures and records the signal from the detector over time.

Figure 1 A schematic of typical set up for GC analysis

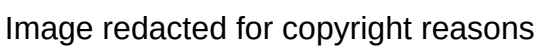

Image source: http://www.scq.ubc.ca/in-the-name-of-fair-game/ [Accessed 17th July 2013]

1.5 Electronic nose and GC/GCMS technology for VOC detection in urine

The Osmotech Microbial Analyzer (OMA) was the first commercially available system to analyse bacteria from urine based on volatile analysis [18]. The device consisted of four polymer sensors that respond to different VOCs released from urine. A carousel of sample vials were kept at a constant temperature. The sample headspace (area above the sample where gases

collect) was delivered across the sensor array for 3 minutes. The sensors were then allowed to recover before humid nitrogen was passed over the array for a 4 minute wash. The resistance of each sensor was measured during the sample period and the change from initial resistance was calculated. Culturing was still necessary for approx. 5 hours and this probably attributed to its lack of commercial success.

GC/MS studies have shown ammonia and acetic acid can occur in the urine headspace of UTI infected patients. Bacterial urease enzymes break down urea to ammonia and this can be used as a biomarker for the presence of bacteria in urine. However not all bacteria break down urea which means that other biomarkers need to be found [19].

This reported research shows there is scope for VOC analysis to be further exploited for disease diagnosis.

1.6 Gas sensors for volatile detection

All gas sensors are based on material(s) that change their physical/electrical characteristics with a vapour/gas. For instance, the physical characteristic change could be based on colour. Also it is desirable for this characteristic to be reversible, i.e. when the gas isn't present the material reverts back to its former state.

1.7 Characteristics of metal oxide sensors for volatile detection

The gas sensor presented in this thesis is metal oxide based. The electrical resistance changes reversibly when exposed to volatiles. Tin oxide is a common material for sensors, however its resistance at room temperature is incredibly high (so high it cannot be measured readily). However on heating, the electrical resistance decreases significantly. A typical sensor operating at 400°C would have a resistance of about 100,000Ω. Volatiles initially adsorb onto the metal oxide surface and change the flow of electrons from the cathode to the anode. At this high temperature a catalytic oxidation of the volatile typically occurs i.e. it reacts with the metal oxide irreversibly. This is akin to burning the volatile. Burning is the addition of oxygen to the volatile. The oxygen atoms come from the atmosphere and importantly from the metal oxide. The removal of oxygen from the metal oxide has a significant effect on its resistance, making it much less resistive and therefore more conductive. For instance tin oxide has a formula SnO_2, and with volatiles present it may convert to e.g. $SnO_{1.8}$ increasing the ratio of metal to oxygen. An increase in conductivity would be expected because the tin oxide is now more metallic. Once the volatile has left, the tin oxide will regain the extra 0.2 oxygen atoms from the atmosphere. Another characteristic of metal oxide sensors is they require a conditioning period (in excess of 30 days) prior to use for volatile detection, where the sensor is heated to operating temperature 24 hours a day with a constant flow of air passing over the surface.

1.8 Design of commercial metal oxide gas sensors

A key electronic aspect of a gas sensor is a device that changes its electrical resistance reversibly when it comes into contact with a gas. The active part of the sensor is a metal oxide that requires electrode contacts to measure the resistance change. A typical example is the Figaro TGS 813 seen in the figure 2. The substrate of this type of gas sensor is an alumina ceramic tube upon which two gold electrodes are printed. Generally gold alloy leads are attached to each electrode using the same gold paste, the leads acting as stays to support the electrodes. Tin oxide is applied over the two electrodes in the form of a paste which is made by adding water to the tin oxide. Typically alumina powder is also added to the tin oxide to improve the ceramic strength of the sensor. The cylinder is then placed in a furnace and sintered at a high temperature. A heater coil is then inserted inside the ceramic cylinder to enable the sensor to be heated.

Figure 2 Figaro TGS 813 gas sensor

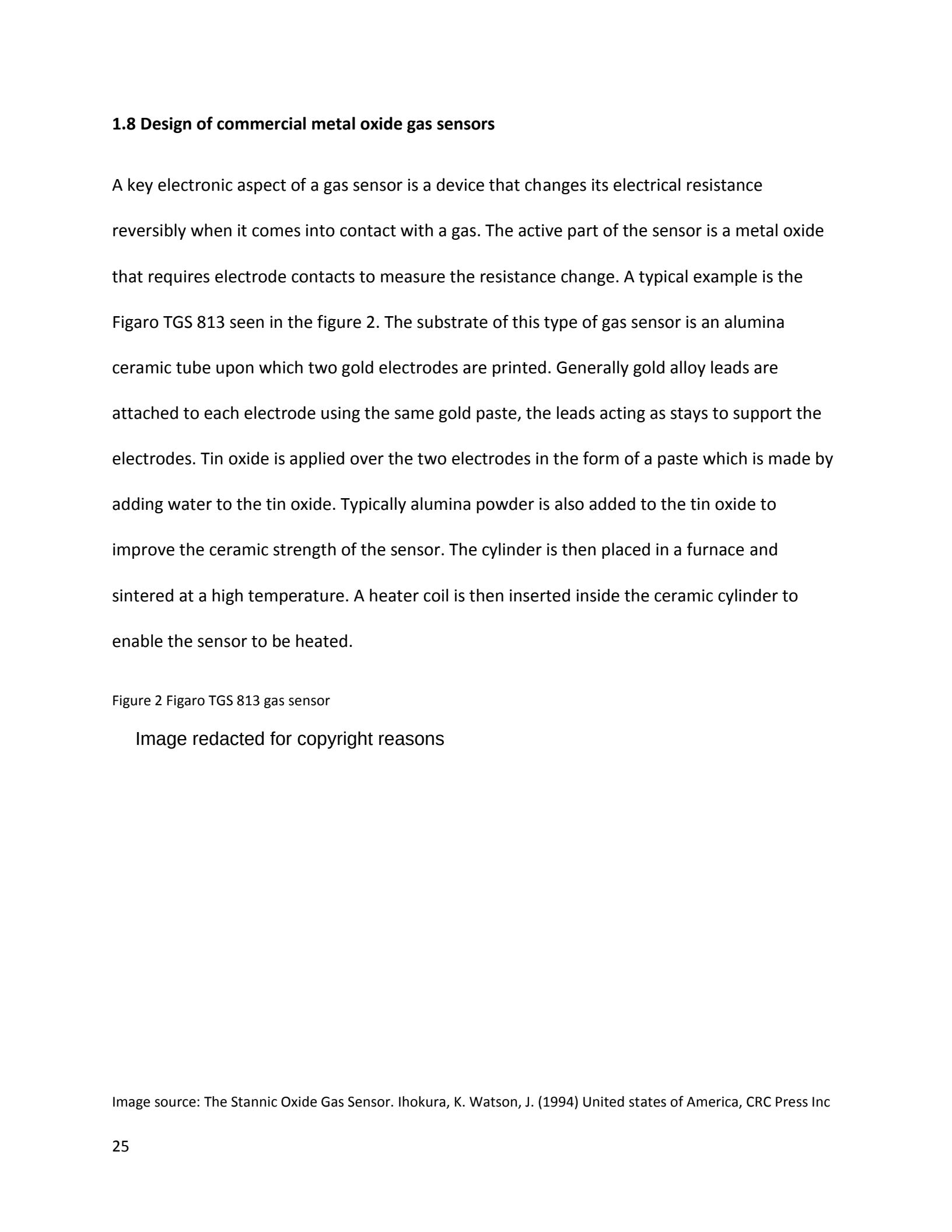

Image source: The Stannic Oxide Gas Sensor. Ihokura, K. Watson, J. (1994) United states of America, CRC Press Inc

Another gas sensor design could be a ceramic substrate with an integrated heater element. This might be screen printed onto the back of the substrate with interdigitated metal electrodes printed on the front. The metal oxide material would then be applied on top of the interdigitated electrodes and would be heated by the heater element on the reverse side of the substrate, see figures 3 and 4.

Figure 3 Heater element printed on the back of a ceramic substrate.

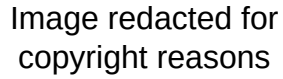

Figure 4 Interdigitated electrodes printed on the front of a ceramic substrate.

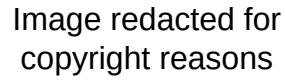

Image source: Google patents; Solid State Sensor Element. US 4307373 A. Johnston, J.S. Rosemount Engineering Company Limited

1.9 The application of electrical components through screen printing techniques

Screen printing is considered a versatile technique that is used to deposit thick film structures onto low cost, flexible and rigid substrates.

Screen printing was first patented in England by Samuel Simon in 1907. Regarded as one of the most versatile, cost effective and high quality printing process [20], screen printing has a wide variety of applications in a range of industries, some of which include glass and furniture design, sign making, ceramics, textiles, automotives and electronics.

Screen printing uses a stencil that is attached to a fine woven mesh (the “screen”) that has been stretched over a frame. The ink or paste is transferred using a squeegee (a type of blade) through the portion of the mesh not masked by the stencil and is deposited directly onto the substrate lying beneath it [21]. Figure 5 illustrates this process in its 3 most basic stages, the top image shows the screen flooded with ink, the middle image shows the squeegee pushing ink through the mesh and the bottom image shows the deposition of ink on the substrate.

Figure 5 Schematic of the basic screen printing process.

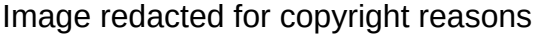

Image source: http://www.gwent.org/gem_screen_printing.html [Accessed 16 July 2013]

1.9.1 Screen mesh types

The purpose of the screen mesh is to provide support for the structure of the stencil and allow the free passage of the printing medium.

Types of mesh

1. Synthetic fibres such as polyester or nylon are now extensively used as they can produce very fine woven meshes. They also have a high tear resistance and a good resistance to extension, making them stable under tension [22].

2. Metal meshes like stainless steel are unaffected by humidity and have a better dimensional stability compared to other materials. They will retain their tension almost indefinitely whereas all conventional synthetic materials have a tendency to lose tension over time [23].

The type of mesh used for printing electronic components depends greatly on the properties of the ink i.e. for conductive inks a mesh count between 230/inch -500/inch and for resistive inks a mesh count between 200/inch – 400/inch is usually used [24].

1.9.2 Inks for screen printing

All inks or pastes consist of two main ingredients; an active element i.e. a pigment or precious metal and a vehicle to convey the active element throughout the process.

Gold or platinum are the preferred metals for durable devices (such as gas sensors) due to their high melting points, inertness to oxidation and chemical attack. Regrettably the cost of these precious metals is high, but wastage in screen printing is kept to a minimum by recovering any paste that is not deposited on the substrate. Gold is less preferred for higher temperature applications due to its lower melting point (1060°C) as opposed to platinum which has a much higher melting point (1700°C). Commercial inks are now available for screen printing bespoke gold and platinum electrodes.

Inks formulated for screen printing electronic components are very viscous at rest, (0.5-5Pa·s) [25] as they contain a high solids content (of around 80%). A typical film thickness of 5-25µm is achieved using this process [24].

1.9.3 Substrates for screen printing

A wide range of materials can be used as substrates for screen printing e.g. ceramics, fabrics, glass, plastics, paper and metal [26]. The substrate selection should be made with consideration for its application and post printing process to ensure that no distortion of the pattern occurs.

1.10 Alternative printing methods used to fabricated electrical components

Other printing methods commonly used in the field of printed electronics are; offset lithography, gravure printing and flexography printing. A wide variety of materials can be deposited using these processes such as conductors, dielectrics, resistors, and semiconductors [27].

1.10.1 Offset lithography

This process uses printing plate cylinders to transfer an image onto a flat substrate. The plate cylinder is chemically treated so that only image areas (such as type, shapes and other elements) will accept ink. Water and ink is applied to the plate cylinder. Because of the chemical treatment, ink only adheres to the image areas, which reject the water. Areas without images reject the ink. The plate is then rolled onto a rubber cylinder applying the inked area, and in turn the rubber cylinder (or "blanket") applies the image to the substrate (see figure 6) [27]. The system is "offset" because the plate does not come in direct contact with the substrate, which preserves the quality of the plate. Ink viscosity for this process is generally between 30-100Pa·s with a typical film thickness of 0.5-2µm [25].

Figure 6 Schematic of offset lithography printing process.

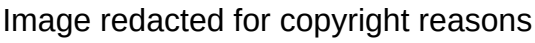

Image source: http://www.offsetprintingtechnology.com/sub-categories/offset-lithography/ [Accessed 16 July 2013]

1.10.2 Gravure printing

In gravure printing, the image is made up of small holes/cells applied to the surface of the printing plate. The holes are filled with ink and any excess is removed by a doctor blade.The substrate comes into contact with the ink in the holes when it is pressed against the plate (see figure 7) [28]. Ink viscosity for this process is generally between 0.01-0.2Pa·s with a typical film thickness of 0.5-2μm [25].

Figure 7 Schematic of gravure printing process

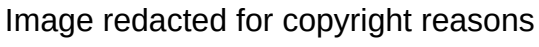

Image source: http://stephmeadmedia.wordpress.com/2012/11/17/printing-methods/ [Accessed 16th July 2013]

1.10.3 Flexography printing

Flexography (Flexo) printing uses a raised image printing plate. Photopolymer or rubber plates are used to transfer the image. As the plate cylinder rotates, it comes in contact with an ink roller, which inks the raised portion of the printing plate. The plate cylinder then transfers the ink to the substrate (see figure 8) [27]. Ink viscosity for this process is generally between 0.05-0.5Pa·s with typical film thickness of 0.5-2μm [23]

Figure 8 Schematic of flexographic printing

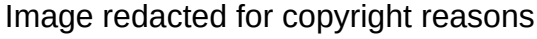

Image Source: http://www.prismpak.com/Printing-Options-s/103.htm [Accessed 16th July 2013]

1.11 Application of electronic components through direct-write techniques

The term 'direct-write' describes a group of additive fabrication techniques that enable the deposition of electronic components and functional/structural patterns onto substrates without the use of masks or resists (unlike traditional printing techniques). It can be incorporated directly with CAD/CAM (computer aided design/computer aided manufacture) software enabling designers to cost effectively prototype new products. Variations of the direct-write technique offer a variety of substrate choice and deposition materials with a range of viscosities [29].

Direct-write techniques were developed in order to provide low cost, rapid manufacturing and shorter time-to-market in the electronics industry. There is an overall reduction in environmental impact due to less waste and a more effective use of materials.

Once material deposition has been completed, thermal post processing is often needed to increase electrical conductivity properties and to ensure optimum performance of the deposited material. This is done either by conventional sintering methods or for low temperature substrate materials a laser is used to locally heat the deposited material without affecting the substrate. Most direct-write techniques can be classified in one of four categories: (1) drop-based direct-write (2) filament based direct-write (3) tip based direct-write and (4) laser based direct-write [30].

Drop based direct-write is a liquid dispensing process where droplets of material are jetted from a single or multiple nozzle(s) onto a substrate. Examples of this process include Ink jet printing and the Aerosol Jet process [31].

Filament based direct-write is a liquid dispensing process where a continuous flow of material is deposited onto a substrate. Examples of this process include MicroPen and nScryp [32].

Tip based direct-write is so named as due to the resemblance this process has to the transfer of ink from quill to paper. The tip is first coated with a solid form of the material and when the tip is heated up the material melts and flows over the tip onto the substrate [33].

Laser beam direct-write techniques rely upon a laser to deposit materials onto substrates. Examples of this process include laser guided direct-write (LGDW) (see figure 9) and flow

guided direct-write (FGDW) (see figure 10). In these techniques a liquid precursor is first transformed into an aerosol which is then introduced into the deposition devices and focused by the optical and hydrodynamic forces (that occur due to momentum transfer between the laser beam and aerosol particles) into a narrow beam. This is then either directly deposited onto the substrate (LGDW) or gets passed through a guidance fibre before being deposited onto the substrate (FGDW) [34].

Figure 9 Schematic of laser guidance direct-write system (LGDW)

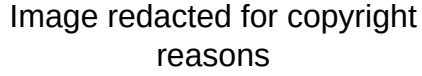

Figure 10 - Schematic of flow guided direct-write system (FGDW

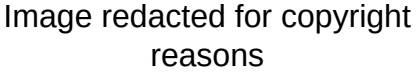

Image source: http://plaza.ufl.edu/yongh/Edu_Biomanufacturing.htm [Accessed 16th July 2013]

Laser induced forward transfer (LIFT) is another example of laser beam direct-write. A thin layer of the deposition material is first coated onto a transparent support which is then lined up so that the coated side of the support is facing the substrate. When laser energy is focused onto the support, the deposition material beneath it will vaporise and fall on to the substrate (see figure 11) [35].

Figure 11- Schematic of laser induced forward transfer (LIFT)

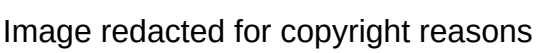

Image source: http://www.orc.soton.ac.uk/lift.html [Accessed 16th July 2013]

1.11.1 Disadvantages of direct-write techniques

Whilst these processes enable on the fly additions/amendments to components, direct-write techniques are still far away from being fully implemented commercially. One of the hurdles these techniques have yet to overcome is manufacturing conductive inks that are chemically and physically stable, capable of drawing patterns with good conductivity and adhesion to substrates [36]. At present there is little need to make bespoke electronics in industry. Alternative methods like screen printing, offer simple, cheap and reliable solutions for the mass manufacture of electronic components.

1.12 Application of thin films through physical vapour deposition methods

Physical vapour deposition is a method that utilises the condensation of a vapour onto a substrate. In general these processes require a substrate which can be heated for better process control (such as uniformity), a target containing the material to be deposited and a source of energy used to convert the material into a vapour [37]. Benefits of this process include high chemical purity of the deposited film, good adhesion between substrate and coating material, layers of uniform thickness with the option to deposit multiple layers [38].

1.12.1 Vacuum evaporation

The source material is heated in a vacuum (10^{-5} torr) until evaporation occurs, upon which atoms from the evaporated material are sent out in all directions forming a thin film on the substrate surface [39]

Figure12 Schematic of vacuum evaporation

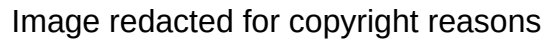

Image source: http://electriciantraining.tpub.com/14186/css/14186_30.htm [Accessed 17th July 2013]

1.12.2 Sputtering

High energy ions are generated and directed at the source material resulting in the sputtering of atoms. These atoms are then transported to the substrate through a region of reduced pressure, condensing on the substrate to produce a thin film [40].

Figure13 Schematic of sputtering process

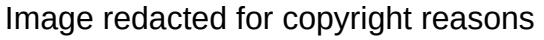

Image source: http://www.gdiy.com/projects/thin-film-sputtering-machine/ [Accessed 17th July 2013]

1.13 Welding of fine wires to sensor substrates

Electronic components often require the joining of fine wires to integrate them into a circuit/device. Sometimes components are joined to a "mount" i.e. a transistor can or a pin header, allowing easy installation to the desired device.

1.13.1 Requirements for sensor operating at high temperature

The choice of electrical connectors for high temperature sensors (e.g. operating around 450°C) is critical to the success of the sensor device, as a failure of the bond means a failure of the device. Some sensors can be operational for years at a time which requires electrical connecters that can withstand high temperatures in order to match the life span of the sensor. The electrical wires also need to be resistant to oxidation as most sensors operate in air. Also the wires need to be very thin (in order to minimise heat conduction from the sensor) and highly electrically conductive. In most cases wires need to be bonded to the sensor substrate and to a sensor mount. Below are common examples of micro-joining techniques.

1.13.2 Micro friction stir welding

Micro friction stir welding is a solid-state joining process, which can be used to join traditionally difficult materials such as aluminium [41].

The process uses a rotating, non consumable weld tool that plunges into the base material and moves forward. Friction heat caused by the rotating pin creates a plasticised tubular shaft around the pin. Pressure provided by the weld tool forces the plasticised material to the back of the pin, cooling and consolidating (see figure 14).

Figure 14– Schematic of Micro frication stir joining process

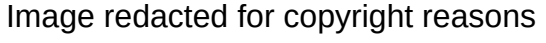

Image source: http://www.twi.co.uk/technical-knowledge/published-papers/developments-in-micro-applications-of-friction-stir-welding/ [Accessed 17th July]

1.13.3 Resistance welding

Resistance Welds are created between materials by applying localised pressure and resistance heating by applying a high electric current, usually with copper electrodes (see figure 15) [42].

Figure 15 – Schematic of resistance welding process

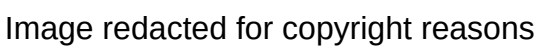

Image source: http://www.cakitches.com/books/spot-welding.html [Accessed 17th July 2013]

1.13.4 Parallel gap resistance welding

Parallel gap resistance welding is the process of bonding two parts together by placing both electrodes against the same surface on just one part. Current flows from one electrode through the top part and partially into the bottom part, before returning to the power supply via the second electrode (see figure 16) [43].

Figure 16 –Schematic of parallel gap resistance welding

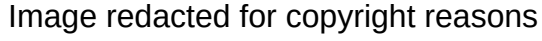

Image source: http://www.miyachieurope.com/technologies/parallel-gap-welding/ [Accessed 17th July 2013]

1.13.5 Welding using lasers

Lasers allow fast processing of materials and thanks to the ability of the laser beam to be focused to a small spot size (down to 7µm with the new generation of fibre lasers), they can be used for micro manufacturing. Processing could be welding, drilling, cutting or ablation of materials (see figure 17) [44].

Figure 17– Diagram illustrating laser welding

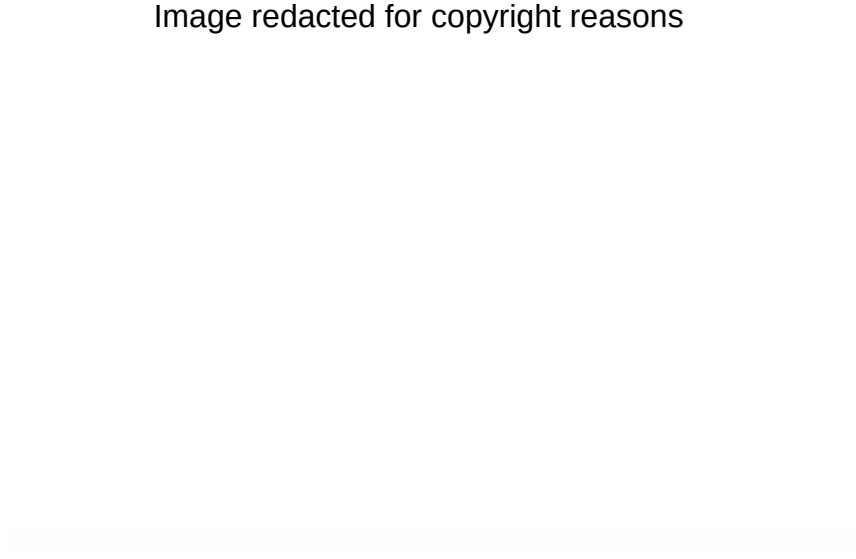

Image source: http://www.joiningtech.com/industry-references/welding-types/laser-beam-welding [Accessed 18th July 2013]

1.13.6 Other joining methods

Adhesives- Silver epoxy resins can be used to join wires to a substrate, these are composed of aromatic di-amines and silver loaded di-epoxides that react together to create a hard resin.

Soldering – Solder is method of joining two pieces of metal by melting them together with another metal. This method is commonly used to bond wires to metal connectors.

Chapter 1 references

1. BCC Research Market Forecasting (2010) Gas sensors and gas metering: applications and markets, www.bccresearch.com/report/IAS012B.html, 09.03.11
2. Figaro Engineering Inc (2003-2008) Company profile, http://www.figarosensor.com/about.html, 22.08.12
3. *Penrose WR. Stetter JR*. Electrochemistry Encyclopedia (2001) The electrochemical nose, http://electrochem.cwru.edu/encycl/, 22.08.12
4. Alpha M.O.S (2011) Products and Technology: Detection, www.alpha-mos.com/products_technology/electronic_nose.html, 12.03.11
5. Dodd G. Persaud K. (1982) Analysis of discrimination mechanisms of the mammalian olfactory system using a model nose, Nature. Vol. 299, Pgs 352–355
6. Bartlett P. Gardner JW. (1994) A brief history of electronic noses, Sensors and Actuators, B Chemical. Vol. 18–19, Pgs 211–220
7. Nagle TH. Osuna RG. Schiffman SS. (1998) The how and why of electronic noses. IEEE Spectrum. Vol. 35, Issue 9, Pgs 22-34
8. Costello B. Garner C. Probert C. Smith S. Spencer R. Ratcliffe N. White P. (2007) Volatile organic compounds from faeces and their potential for diagnosis of gastrointestinal disease, *The FASEB Journal*. Vol. 21, No. 8, Pgs 1675-1688
9. Bessant C. Buijtels P. Fend R. Klatser PR. Kolk AHJ. Woodman **AC. (**2006) Prospects for clinical application of electronic-nose technology to early detection of mycobacterium tuberculosis in culture and sputum, Journal of Clinical Microbiology. Vol. 44, No. 6, Pgs 2039-2045

10. Fowler D. (2010) MSc Thesis, Analysis of volatile marker compounds in body fluid samples from patients with gastrointestinal diseases, Cranfield University
11. Chowdrey H. Kodogiannis V. Lygouras J. Tarczynski A. (2008) Artificial odour discrimination system using electronic nose and neural networks for the identification of urinary tract infection, IEEE Transactions of Information Technology in Biomedicine. Vol. 12, No. 6, Pgs 707-713
12. Baker L. Cataneo R. Gleeson K. Greenberg J. Hughes JM. McVay WP. Phillips M. (1999) Volatile organic compounds in breath as markers of lung cancer: a cross-sectional study, The Lancet. Vol. 353, Issue 9168, Pg 1930 - 1933
13. Scully C. Greenman J. (2008), Halitosis (breath odour), Periodontology 2000. Vol. 48, Issue 1, Pgs 66–75
14. Pembroke A. Williams H. (1989) Sniffer dogs in the melanoma clinic? The Lancet. Vol. 333, Issue 8640, Pg 734
15. Bransbury A. Church J. Church S. Church M. Cook A. Guest C. McCarthy N. Willis C. (2004) Olfactory detection of human bladder cancer by dogs: proof of principle study, BMJ. Vol. 329, No. 7468, Pg 712
16. BBC News Health, (2011) Sniffer Dogs detect Lung Cancer, http://www.bbc.co.uk/news/health-14557224, 06.09.11
17. J&W catalogue (1998) Gas Chromatography, http://delloyd.50megs.com/moreinfo/gaschrom.html, 28.08.12
18. The Osmetech Microbial Analyser TM_ Urinary Tract Infection Detector (2001) Osmetech plc, 51 O(k) Premarket Notification

19. Evans P. Persaud K. Pisanelli AM. Travers P. (2006) Monitoring urinary tract infections and bacterial vaginosis, Sensors and Actuators B: Chemical. Vol. 116, Issue 1-2, Pgs 116-120
20. Nelson K. (2010) The Screen Option, Ceram.ind. Vol. 160, No. 3, Pgs 20-22
21. Gwent, Hobby A. (1997) Screen printing for the industrial user, http://www.gwent.org/gem_screen_printing.html, 08.09.11
22. Stephens J. (1996), Screen process printing, 2nd edition, Blueprint Publishers, Pg 6
23. Stephens J. (1996), Screen process printing, 2nd edition, Blueprint Publishers, Pg 14
24. Sefar, Thick film, http://www.sefar.com/htm/609/en/Product-Detail.pdf?Folder=1465762, 24.08.12
25. ICT Sector Focus Report (2010) Printed electronics, http://www.observatorynano.eu/project/filesystem/files/ObservatoryNanoFocusReport_PrintedElectronics.pdf, 23.08.12
26. Printers national environmental assistant centre (1995) Screen printing, http://www.pneac.org/printprocesses/screen/, 22.08.12
27. Jurgen D. (2010) Printed Electronics:Technologies, Challenges and Applications, Palo Alto Research Center, International Workshop on Flexible and Printed Electronics
28. Subramanian V. Sung D. (2008) Gravure as an industrially viable process for printed electronics, Electrical Engineering and Computer Sciences, University of California at Berkeley, Technical report No. UCB/EECS-2008-70
29. Longtin J. Sampath S. Tankiewicz S. Gambino R. Greenla R. (2004) Sensors for Harsh Environments by Direct-Write Thermal Spray, IEEE Sensors Journal. Vol. 4, No. 1

30. Pique A. Chrisey D.B (2002) Direct-write technologies for rapid prototyping applications, Academic press. Pg 43-45
31. Hoey JM. Lutrurakmanov A. Schulz DL. Akhatov IS. (2011) A review on Aerosol based direct write and its applications for microelectronics, Journal of Nanotechnology. Pg2
32. Oianwa H. Xiangyou Li. Xiaoyan Z. Zhixiang C. (2008) Study on thick film PTC thermistor fabricated by micro-pen direct writing, Microelectronics Journal. Vol. 39, Issue 12, Pgs 1452 - 1456
33. Pique A. Chrisey DB. (2002) Direct-write technologies for rapid prototyping applications, Academic press. Pg 647
34. Pique A. Chrisey DB. (2002) Direct-write technologies for rapid prototyping applications, Academic press. Pg 39-40
35. Phipps C.R (2007) Laser Ablation and its applications, Springer Science + Business Media LLC. Pg 341
36. Kim NS. Han KN. (2010) Future direction of direct writing, Journal of applied physics. Vol. 108, Issue 10
37. Guo Z. Tan L. (2009) Fundamentals and applications of nanomaterials, Pg100
38. Las positas college (2002) Chapter 14,Thin film deposition process, http://lpc1.clpccd.cc.ca.us/lpc/tswain/chapt14.pdf, 25.08.12
39. AglaSem, Deposition of thin films by thermal evaporation and design of gas sensor alarm, http://aglasem.com/resources/reports/pdf/ProjectonGASSENSOr.pdf, 24.08.12
40. Angstrom Sciences (2010) Sputtering technology, www.angstromsciences.com/technology/sputtering-technology 12.05.11

41. TWI (2001) Micro friction stir welding, http:/www.twi.co.uk/content/tfmicrofsw.html, 23.05.11

42. TWI (2001) Resistance welding, http:/www.twi.co.uk/content/resistance_index.html, 23.05.11

43. Micro joining solutions, Steinmeier D. (2010) Resistance welding – parallel gap welding basics, www.microjoining.com, 25.08.12

44. TWI (2001) Laser welding, http:/www.twi.co.uk/content/laser_welding.html, 23.05.11

Chapter 2 – Sensor construction

2.1 Introduction: Design and fabrication of a new mini gas sensor

Requirements outlined for the OdoReader device specified that sensors were to have a low heater resistance at room temperature, be able to withstand high operating temperatures (around 450°C), be reproducible, robust and finally compatible with existing components. Sensors with required specifications were not commercially available making it essential to fabricate sensors in-house. This necessitated a multi step fabrication process, the key parts of which are detailed below.

- Generation of sensor design using CAD (computer aided design) software
- Patterns converted into monochrome image for screen production
- Generation of laser score path (using CAD software) for substrate
- Screen printing of the sensor design onto the scored substrate
- Separation of sensor substrate
- Application of sensor layer
- Resistance welding of gold wire from sensor substrate to holding device
- Sensor unit assembly

Screen printing is a robust and well tried process used in the fabrication of gas sensors. The work here used screen printing for two key aspects of the sensor; the heater track and the interdigitated electrode track.

2.1.1 Substrate material selection

Alumina was picked as a substrate material due to its inertness at high temperatures, the option of laser scoring (for substrate separation) and the ease to which metals adhere.

2.1.2 Inks for screen printing

Gold was chosen for the interdigitated electrode material due to its inertness and its relatively high melting point despite its very high cost. Platinum was chosen for the heater material for the same reasons, but was selected over gold for this feature due to its much higher melting point (1772°C as compared to gold with a melting point of 1064°C).

2.2 Sensor types

Two types of sensor designs were produced; type A, sensor substrates designed to be used in card edge connectors and type B sensor substrates designed to be suspended on transistor cans by bonded fine wires.

2.3 Type A sensors for card edge connectors

Card edge connectors are devices that provide electrical connections with single or double sided printed circuit boards. The contacts are made of metal and are plated with metals such as gold, nickel copper and silver to improve conductivity and prevent rust and corrosion. Plastic terminals commonly house the contacts and some varieties are available that are especially

suited for high temperature operation (see figure 18). The distance between the contacts (the contact pitch) can range from as small as 0.5mm to as large as 2.84mm.

Figure 18 - A double sided edge connector supplied by Sullins electronics

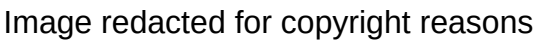

Image source: http://www.digikey.co.uk/product-detail/en/EBM22DRAS/S3350-ND/927302 [Accessed 17th July 2013]

Type A sensors were printed on rectangular strips of alumina with a heater track on one side and interdigitated electrodes on the other. Two sensor designs were made for this type; A1 and A2. Figures 19 and 20 show these sensor substrate designs inserted into card edge connectors.

2.3.1 Features of sensor design A1

A key design feature sensor A1 (shown in figure 19) was the length of the electrode pads. They had to be long enough to keep the heater element a good distance away from the card edge connector contact to prevent overheating when the sensors are in use. Another key aspect to this design was the decision to print onto very thin (250µm) sheets of alumina. This was to minimise heat flow through the substrate so that low power requirements could be met if the sensors was one day to be used in a portable battery operated system. This sensor was designed to fit into a two sided card edge connector.

Figure 19 – Front and back view of sensor design A1 in double sided card edge connector

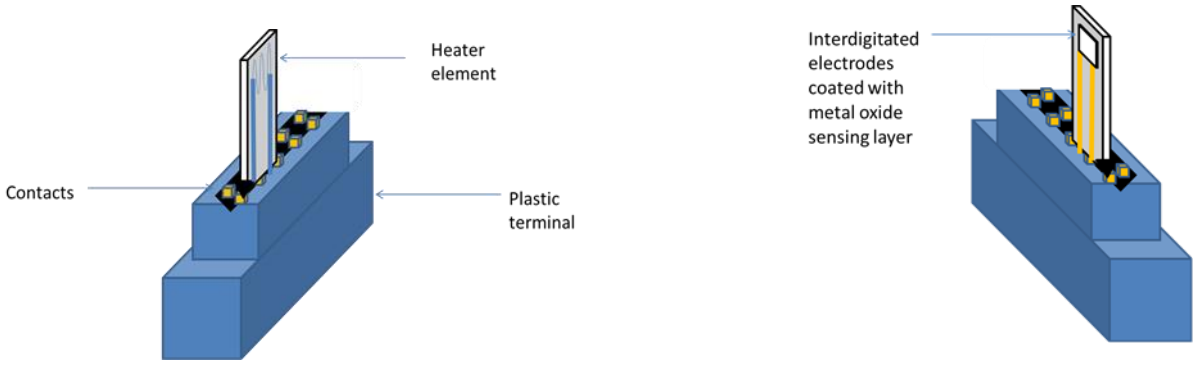

2.3.2 Features of design A2

A key design feature of sensor A2 (shown in figure 20) was the location of the heater element and the interdigitated electrodes. They were positioned in the centre of the substrate (on opposing sides). This sensor was designed to be suspended between two single row edge connecters, so the contact pads of the heater went to one plastic terminal and the interdigitated electrode contact pads went to another.

Figure 20 – Front and back view of sensor A2 in a single sided edge connector

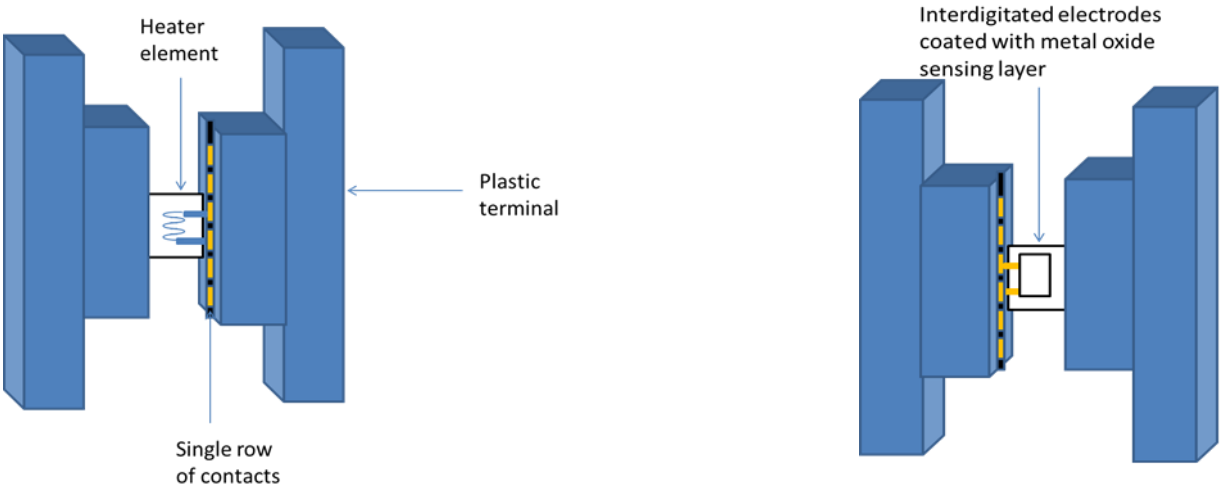

2.3.3 Advantages and disadvantages of type A sensors

The advantage of designing type A sensors is that installing and removing sensors would be relatively easy. There would be no need for specialised wire bonding which would add time and money to the fabrication process.

The disadvantage of type A sensors is the restriction in dimensions of commercially available card edge connectors. Although available in different widths, a company that could supply a card edge connector with a 0.25mm gap between contact row(s) could not be found, meaning that sensor A1 and A2 would not fit securely in the card edge connector. Some companies will custom build edge connectors to specific dimensions, but through discussions with several of them it became clear that the cost of this would be too high. It was decided instead to attempt to increase the thickness of the substrate so that it would fit into a commercially available card edge connector with a width of 0.5mm between contact row(s)

2.3.4 Gold bumping for type A sensors

To increase the thickness of the substrate by 100%, 250µm gold wire was dropped onto the contact pads on the interdigitated side of the substrate. The work here was carried out by Dr Helen Goddin from The Welding Institute.

The thickness of the substrate was successfully increased to 500µm and subsequently fitted securely into a commercially available edge connector. However it required a lot of gold bumps to cover the surface of the electrode pads. There were also concerns that the gold bumps might

flatten over time through repeated insertion and removal from the card edge connector. It was therefore decided that this was not a viable long term option.

2.3.5 Peg connectors for sensor design A2

Sensor design A2 could also be mounted in a pin header with gold peg connectors soldered to the pins. Figure 21 shows this set up - the sensor is located on the right hand side held by 4 gold pegs which are each in turn soldered to a pin header.

Figure 21 – Photograph of sensor A2 in peg connector device

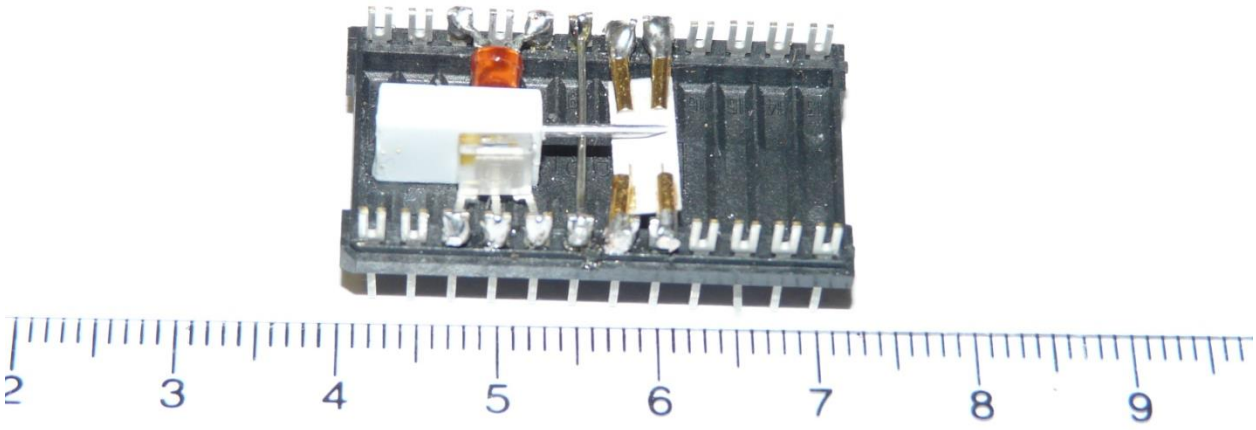

2.3.6 Advantages and disadvantages of peg connectors

The sensor was supported securely by the gold pegs and good contacts were established. However, inserting the sensor between the pegs was fiddly and the pegs needed to be prised apart for the substrate to rest between them. Sometimes the pegs were opened too far and pushing them back together again once the sensor was positioned resulted in the substrate

snapping in half. With repeated use the pegs deformed and wouldn't hold the sensor anymore resulting in the rejection of entire peg connector units.

2.4 Type B sensors – Designing a sensor for wire bonding

Type B sensors were printed on square pieces of alumina with a heater on the one side and interdigitated electrodes on the other. A layer of gold was screen printed on top of contact pads on the platinum heater side of the substrate as it was found that gold wire bonded better to gold ink.

A smaller sized substrate was used for this type of sensor. The substrate was thicker than type A sensors but had a thermal mass that was considerably less. Figure 22 shows this sensor design mounted on a transistor can.

Figure 22– Schematic of type B sensor mounted on a transistor can

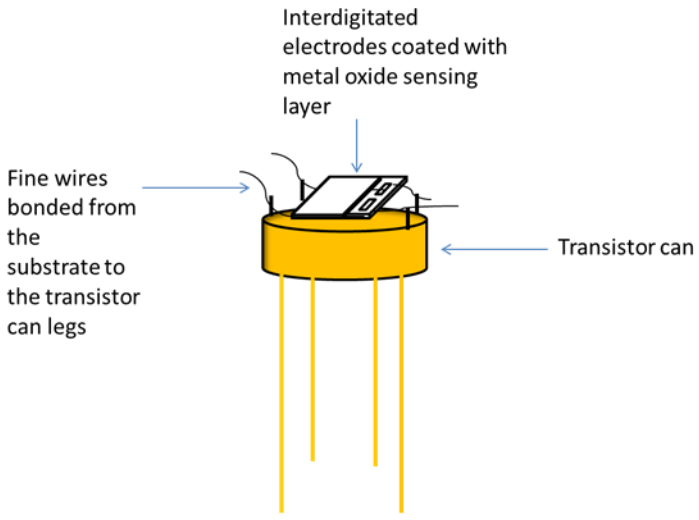

2.4.1 Advantages and disadvantages for sensors designed for fine wire bonding

Suspending the sensor by fine wires results in less heat loss compared to type A sensors. The smaller sized substrate reduces power consumption which is of particular importance for a battery operated portable system. The low heat emissions are also beneficial for compact systems housing complex electronics.

The disadvantage of fine wire bonding is the added cost and time to the fabrication process. There is also the risk of the wire breaking due to thermal fatigue, resulting in a loss of contact with the transistor can.

2.5 Sensor designs

Rhino version 4 was used to generate the files for these sensor designs.

Type A sensors consisted of two patterns where as type B sensors had three for fine wire bonding purposes.

Type A sensors:

1) Gold interdigitated electrodes - printed on one side of an alumina substrate
2) A platinum heater - printed on the opposite side of the alumina substrate

Type B sensors

1) Gold interdigitated electrodes - printed on one side of an alumina substrate
2) A platinum heater - printed on the opposite side of the alumina substrate

3) Gold contact pads – printed over the top of the platinum heater pads

Tables 2 – 8 show the dimensions all 3 sensor designs followed by a CAD drawing of each side of the substrate. These designs were drawn at UWE with the help of Dr Peter Walters.

2.5.1 Type A1 sensor design

Substrate size – 15mm x 3.5mm

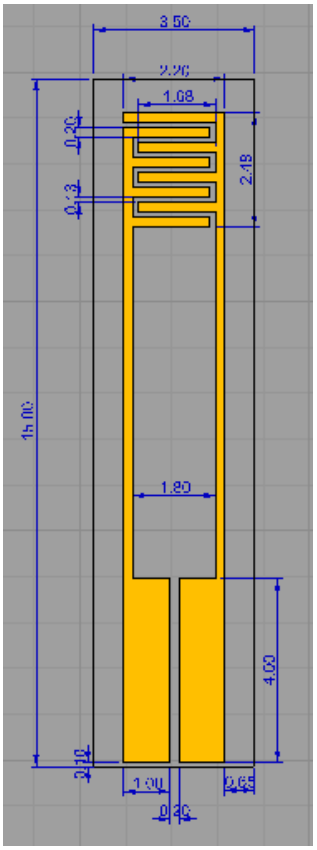

Table 2 – Basic dimensions of interdigitated electrode side of sensor

Sensor feature	**Dimensions**
Electrode track width	200µm
Interdigitated gap	130µm
Contact pad width	1000µm
Contact pad length	4000µm

Table 3 – Basic dimensions of heater side of sensor

Sensor feature	**Dimensions**
Heater track width	200µm
Gap between meanders	200µm
Contact pad width	1000µm
Contact pad length	11050µm

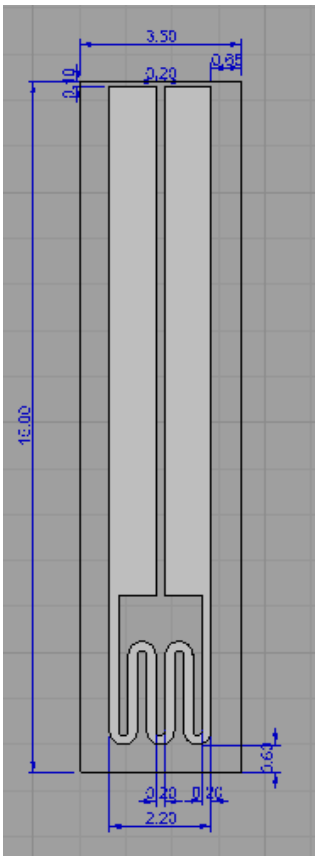

2.5.2 Type A2 sensor design

Substrate size 10mm x 4mm

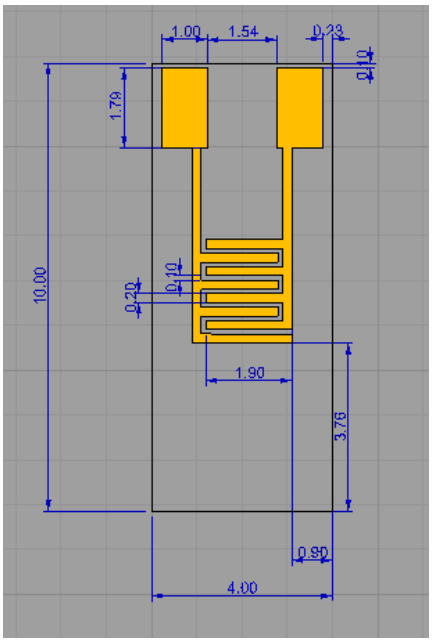

Table 4 – Basic dimensions of interdigitated electrode side of sensor

Sensor feature	**Dimensions**
Electrode track width	200µm
Interdigitated gap	100µm
Contact pad width	1000µm
Contact pad length	1790µm

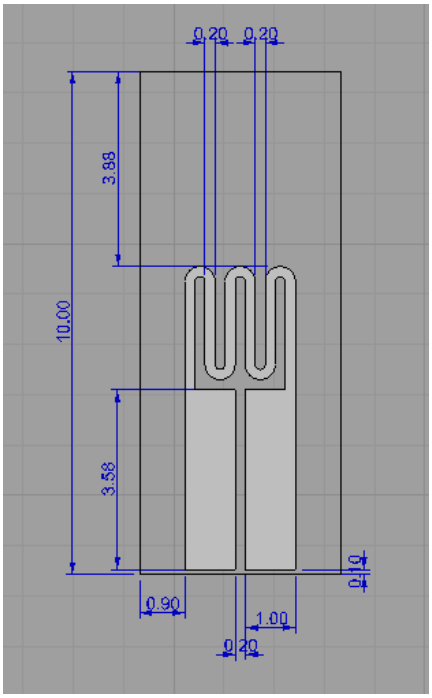

Table 5 – Basic dimensions of heater side of sensor

Sensor feature	Dimensions
Heater track width	200µm
Gap between meanders	200µm
Contact pad width	1000µm
Contact pad length	3580µm

2.5.3 Type B sensor design

Substrate size- 3mm x 3.089mm

Table 6 – Basic dimensions of interdigitated electrode side of sensor

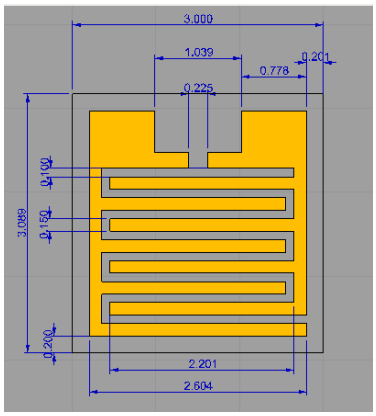

Sensor feature	Dimensions
Electrode track width	150µm
Interdigitated gap	100µm
Contact pad width	778µm
Contact pad length	499µm

Table 7 – Basic dimensions of heater side of sensor

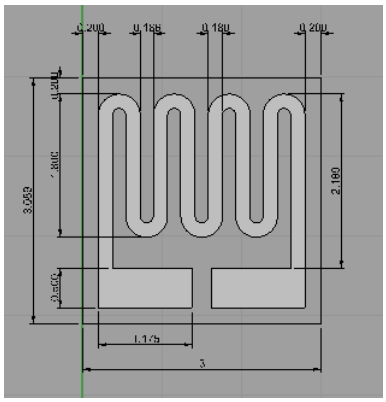

Sensor feature	Dimensions
Heater track width	180µm
Gap between meanders	166µm
Contact pad width	1175µm
Contact pad length	500µm

Table 8 – Dimensions of contact pads for heater side of sensor

Sensor feature	Dimensions
Contact pad length	500µm
Contact pad width	1175µm

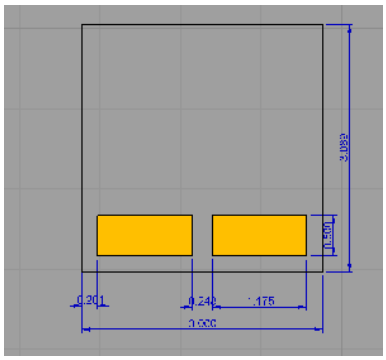

2.5.4 Overview of sensor designs

Two types of sensor substrates were designed; type A sensors for card edge connectors and type B sensors for fine wire bonding to transistor cans. These designs were then sent to ELS (a screen printing company) to be printed onto alumina substrates (see section 2.11 for details) so that an initial assessment of the heater element could take place.

2.6 Heater element testing of type A sensors

To test the functionality of the platinum heater of sensors A1 and A2, a voltage was applied to the contact pads on the heater side of the sensor substrates. The voltage was increased at 1V increments until 8 volts was reached and then at 0.25V increments until the temperature of the sensor substrate reached at least 450°C. A thermocouple (Type K thermocouple) was used to measure the temperature and was positioned at the centre of the heater element a few millimetres away from the surface).

Two wires were connected to the contact pads on the heater side of the sensor substrate. Silver epoxy (RS silver loaded epoxy adhesive, 10g 2 vials, stock number 186-3616) was applied to the end of the wire (Maplins), and held in place until the adhesive cured. The sensor substrate was then secured in a clamp stand and held by the wires joined to the contact pads. This method of joining was meant as a temporary solution, to enable initial tests to take place.

2.6.1 Results and discussion for sensor A1

Figure 23- Voltage/temperature characteristics for sensor type A1

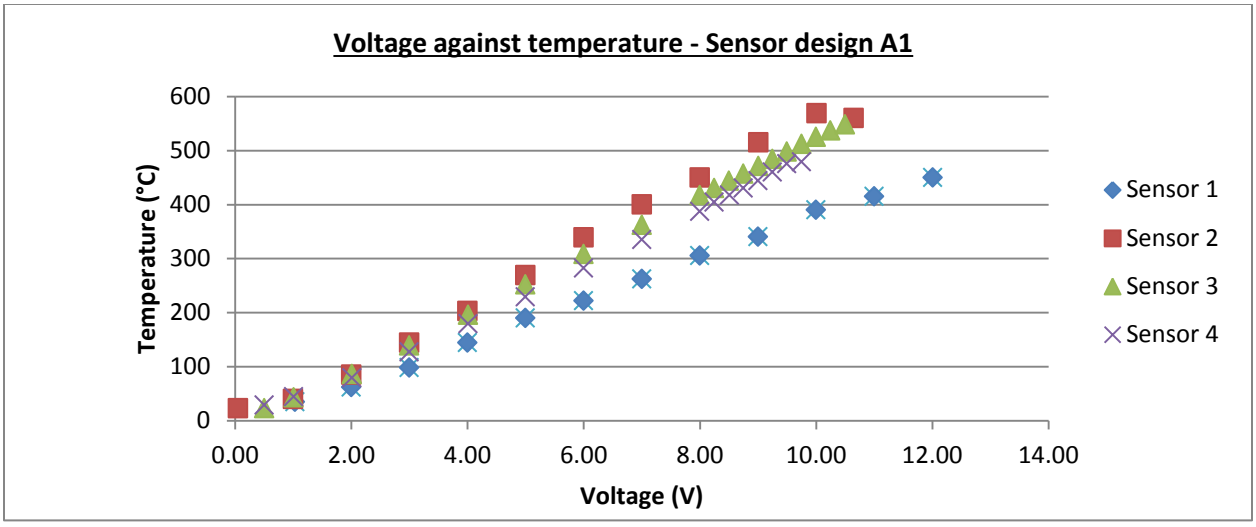

Figure 23 shows the voltage input against temperature measurements from four type A1 sensors. All four sensors reached the desired operating temperature of 450°C. This temperature was exceeded for sensors 2, 3 and 4. The graph illustrates that the very high operating temperature of 596°C is achievable.

2.6.2 Results and discussion for sensor A2

Figure 24 - Voltage/temperature characteristics for sensor type A2

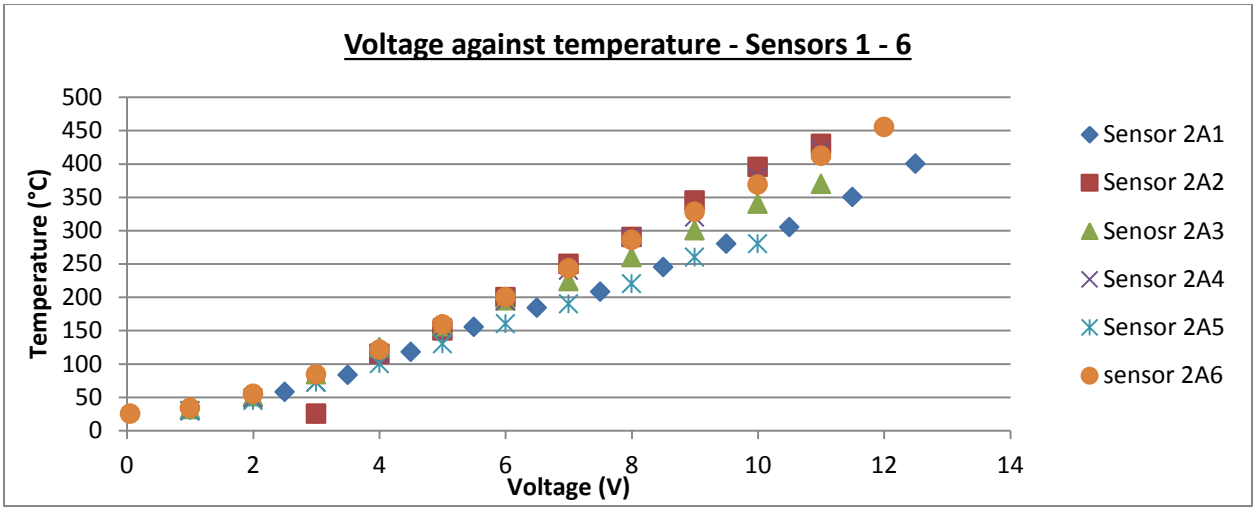

Figure 24 shows the voltage input against temperature measurements from 6 type A2 sensors. The results from these sensors suggest that they would operate at temperatures up to 370°C. The sensors catastrophically failed when temperatures exceeded 370°C snapping in half across the centre of the heater element. For this reason, this design was abandoned.

2.7 Heater element testing of type B sensors

Type B sensors were tested once welded to transistor cans (a more extensive study investigating the functionality of the heater element can be found in section 2.19). An increasing voltage was applied to the pins of the transistor can and the temperature was monitored using a thermocouple in a similar fashion to sensor A1 and A2. This design was found to be particularly suitable for high temperature operation. The voltage was increased until the

gold interdigitated electrodes melted, suggesting an operating temperature at the melting point of gold (greater than 1000°C) could be potentially be used.

2.8 Selection of type B sensor

The combination of B type sensors and the transistor can provide a versatile combination in that both the transistor can and sensor could be soldered to a variety of different platforms/devices. This sensor design fulfilled the requirements specified for the OdoReader device and for that reason it was selected. This sensor design also benefits from reduced power consumption and lower heat emissions due to the smaller size of the substrate (compared to type A sensors). This is would be a desirable feature if the OdoReader device was to one day be a battery operated, portable system.

2.9 Batch production of type B sensor

2.9.1 Designs on to acetate for screen production

Each design was placed onto a grid (representing the score lines of the alumina substrate) and converted into a monochrome image. The images were sent to Philips Digital where they were transferred onto a transparent film (Agfa – photo plotting film) using a photoplotter (Printer – MIVA tech 2516E t3). The films were then sent to MCI precision screens Ltd where each design was transferred on to a separate screen.

2.9.2 Details of screen manufacturer

Supplier of service- MCI precision screens Ltd

Address – Saxon way industrial estate, Melbourn, Nr Royston, Hertz, SG8 6DN

Format required for image file- DWG

Screen size- 6x8 inches

Mesh material for the gold interdigitated electrode screen- V mesh 330

Mesh material for the platinum heater and gold pad screens – Stainless steel 325 mesh

Screen tension – Stainless steel 25-26, V mesh 24-26

Emulsion thickness - 10µm

Emulsion type – E40

2.9.3 Ink formulation – Gold and Platinum

It was decided to use commercial formulations of gold and platinum inks for the screen printing process. Three of the main suppliers of conductive inks in the UK are Dupont, ESL and Gwent Electronics. ESL and Gwent were favoured as they provided ink and a screen printing service, of these ESL was selected due to their considerable experience in printing fine line conductive inks. The details of the exact composition of these inks were commercially sensitive however the general components are listed below;

Gold paste details - ESL Au 8880-0H

TCR of paste- 3000-3500ppm/°C

Approximate solid content- 90%

Paste content - a binder (frit less material) and a printing vehicle

Platinum paste details- ESL 5545

TCR of paste – 3500ppm/°C

Approximate solid content – 75%

Paste content – a glass frit and a printing vehicle

2.9.4 Laser scoring and supplier information of alumina substrates

The laser scoring process uses a focused spot of laser energy to remove alumina material to a specified depth. The benefit of laser scoring is that it is a precise and high speed process that can be performed on wide variety of materials. The laser follows a pre-determined path (designed using CAD software), and pulses short bursts of energy to create a type of perforated edge. This enables the alumina to be snapped along a score line with ease and control.

Alumina substrates were purchased from Laser Cutting Ceramics Ltd, Catley Road, Sheffield, S9 5JF. The substrates were processed to our specifications, listed below:

- Size of substrate sheet – 50mm x 54mm
- Thickness of substrate -0.635mm
- Score depth -75%
- Grid dimensions -3.09mm x 3mm

- Number of rectangles -16 x14

The above specifications were checked using a representative sample at UWE and found to be accurate. The score depth was checked using a micro-spectrophotometer (MSP). A micrometer was used to check the size and thickness of 6 sensor substrates. Ten measurements were taken from each sensor for the width, length and thickness. As can be seen in tables 9 and 10 there is good reproducibility in achieving the desired dimensions. The main reason for the variation is due to the perforated edge caused by the laser when the substrate was laser scored. Table 11 shows that the substrate thickness varies very little from sensor to sensor. Of the 60 thickness measurements taken, a S.D. from the mean thicknesses of 0.005mm was calculated, again showing good reproducibility.

Table 9 - 10 length measurements of 6 type B sensor substrates

Length (mm)	1	2	3	4	5	6	7	8	9	10	Mean	Overall Mean
Sensor 1	3.15	3.16	3.03	3.06	3.09	3.04	3.09	3.14	3.06	3.05	3.09	3.09
Sensor 2	3.11	3.09	3.10	3.10	3.09	3.07	3.14	3.10	3.09	3.09	3.10	
Sensor 3	3.13	3.11	3.16	3.12	3.09	3.09	3.11	3.12	3.10	3.07	3.11	
Sensor 4	3.10	3.09	3.13	3.14	3.07	3.05	3.12	3.07	3.12	3.11	3.10	
Sensor 5	3.09	3.02	3.03	3.02	3.03	3.11	3.10	3.04	3.12	3.04	3.06	
Sensor 6	3.09	3.07	3.11	3.10	3.05	3.06	3.04	3.06	3.20	3.09	3.09	

Table 10 - 10 width measurements of 6 type B sensor substrates

Width (mm)	1	2	3	4	5	6	7	8	9	10	Mean	Overall Mean
Sensor 1	2.97	2.98	2.93	2.94	2.93	2.97	2.98	2.99	2.94	2.94	2.96	2.97
Sensor 2	3.03	2.97	2.96	2.98	2.97	2.94	2.94	2.94	2.96	2.94	2.96	
Sensor 3	2.98	2.99	3.00	3.00	2.98	2.98	2.99	2.98	2.99	2.99	2.99	
Sensor 4	2.95	3.01	2.96	3.01	2.96	2.95	2.95	2.95	2.98	2.97	2.97	
Sensor 5	2.95	3.01	2.96	3.01	2.96	2.95	2.95	2.95	2.98	2.97	2.97	
Sensor 6	2.98	2.96	2.98	2.93	2.95	2.95	2.96	2.95	2.93	2.93	2.95	

Table 11 - 10 thickness measurements of 6 type B sensor substrates

Thickness (mm)	1	2	3	4	5	6	7	8	9	10	Mean	Overall mean
Sensor 1	0.57	0.56	0.58	0.6	0.58	0.57	0.57	0.57	0.57	0.62	0.58	0.60
Sensor 2	0.58	0.63	0.56	0.56	0.57	0.60	0.58	0.57	0.58	0.57	0.58	
Sensor 3	0.58	0.56	0.56	0.58	0.57	0.57	0.56	0.56	0.57	0.57	0.57	
Sensor 4	0.58	0.56	0.57	0.56	0.57	0.57	0.61	0.57	0.58	0.59	0.58	
Sensor 5	0.60	0.56	0.56	0.57	0.56	0.58	0.57	0.59	0.57	0.57	0.57	
Sensor 6	0.57	0.59	0.58	0.57	0.56	0.57	0.57	0.57	0.60	0.57	0.58	

2.10 Separation of alumina sheets

To find the best way of breaking up a scored sheet of alumina into individual substrates, 3 methods were tried.

These were;

- Separation by hand
- Rolling an aluminium rod, covered with thick rubber tubing over the substrate
- Separation using an adjustable spanner to snap off single rows of sensor

2.10.1 Method 1 - Separation by hand

Powder free gloves were worn to minimise contamination of the sensors. A downward force was applied to the un-scored side of the substrate resulting in a controlled fragmentation of the sheets. Repetition of this action successfully separated all the sensor substrates from the alumina sheet.

2.10.1.1 Results

An entire sheet consisting of 224 sensor substrates was separated with no losses. The alumina sheet was easily split in half, but as the fragments got smaller the amount of force required to snap the substrate increased.

2.10.2 Method 2 - Separation by roller

The alumina substrate was placed scored side down on a rubber mat, with sheets of paper positioned on top to protect the substrate from the roller. A pressure was applied to the roller while it was moved backwards and forwards over the substrate to instigate cracking parallel to the movement. The substrate was then turned 180° and this action was repeated.

2.10.2.1 Results

The alumina sheet was broken into fragments of sensor substrates joined together generally in 2's and 4's. Separation of individual sensors substrates was not achieved and a significant amount of powdered alumina was visible on the rubber mat. This suggested that this method was causing considerable damage to the substrates. Although incomplete, this method was significantly faster than hand separation.

2.10.3 Method 3 - Separation by adjustable spanner

An adjustable spanner was used for separation of substrate strips along vertical score lines. Paper-backed tape was applied to the jaws of the spanner to protect the substrate from dirt and uneven pressure.

Similar to separation by hand, this method used a downward force that was applied to the un-scored side of the alumina. The spanner was lined up and secured to the outer side of a chosen score line, with the other hand lined up on the inner side of the score line (holding between the thumb and the index finger). Using the 'spanner holding hand', a downward force was applied to break the substrate.

2.10.3.1 Results

This method allowed a row of sensors to be removed at a time, giving a more structured separation of the substrate. As pressure was only applied to the few sensors on each row (where the spanner was secured), there was minimal damage to substrate.

2.10.4 Conclusion

Methods 1 and 3 provided controlled separation of the alumina sheet with no losses due to uncontrolled cracking. Using both of these methods together, i.e. separation of sensor substrate rows using the spanner technique followed by hand separation of individual sensor substrates, the alumina sheet was quickly and effectively divided. It was for this reasons that these methods were adopted.

2.11 Screen printing the sensors

Screen printing work took place at ESL Europe, 8 Commercial Road, Reading, Berkshire, RG2 0QZ, with John Whitmarsh and Karen Jones Williams. A Dec 1202 screen printing machine was used for all screen printing work.

2.11.1 Printing the gold interdigitated electrode pattern

The interdigitated electrode pattern was printed onto the scored side of the alumina substrate. Gold paste was deposited onto the interdigitated electrode patterned screen. Once aligned with the substrate, a vacuum was applied (to hold the substrate in place) whilst a flood blade dragged the paste over the screen. A squeegee then pushed the paste through the permeable parts of the screen to transfer the ink onto the substrate.

Substrates were dried (120°C-125°C) for 10 minutes and then sintered in a 5 zone belt furnace for 30 minutes reaching a maximum temperature of 850°C (see below for temperature zones of belt furnace).

2.11.2 Printing the platinum heater pattern

The platinum heater was printed on the opposite side of the alumina on the un-scored side of the substrate. The printing process was the same as before, except for the use of platinum paste instead of gold and a heater pattern screen instead of interdigitated electrodes. The substrate was dried (120°C-125°C) for 10 minutes and then sintered in a belt furnace for 60 minutes reaching a maximum temperature of 980°C (see below for temperature zones of belt furnace).

2.11.3 Gold contact pads over the platinum heater pads

The gold contact pads were also printed on the un-scored side of the substrate, directly over the existing platinum contact pads. The process of printing and drying was the same as before and the substrate was sintered in a 5 zone belt furnace for 30 minutes, reaching a maximum temperature of 850°C (as the gold electrodes were).

2.12 Drying equipment times and temperatures

Drying time- 10 minutes

Drying temperature – 120-125°C

Sintering time for gold ink – 30 minutes

Sintering time for platinum ink – 60 minutes

Furnace type - Standard Metri therm 5 zone belt furnace.

2.12.1 Temperature zones of belt furnace for gold paste

Zone 1 – 828°C

Zone 2 –848°C

Zone 3 – 848°C

Zone 4 – 852°C

Zone 5 – 840°C

2.12.2 Temperature zones of belt furnace for platinum paste

Zone 1 – 810°C

Zone 2 – 967°C

Zone 3 – 973°C

Zone 4 – 978°C

Zone 5 – 890°C

2.13 Selection of in-spec. sensors based on heater resistance at 0°C

To determine the overall mean resistance value and standard deviation of 3 sheets of printed substrates, the resistance of 672 heater elements (224 per sheet) were recorded. Two readings were taken (using a digital multimeter UT50-11 supplied by UNI-TREND Group Ltd) to minimise error during the measurement period. The temperature was also measured and recorded for each sensor substrate (using a glass 76mm x 1mm thermometer supplied by Fisher Scientific). It was important that the fluctuations in temperature were factored out, and that a resistance value was calculated for each sensor substrate at one temperature (0°C). Using the temperature co-efficient of resistance (TCR) of the platinum paste the following equation was applied. [Equation reference: Hernández, C.A. and Wilson, J.D. (2009) *Physics Laboratory Experiments* [online]. 7th ed. Usa: Cengage Learning. [Accessed 22 July 2013]

$$R_0 = \frac{R_t}{\{1+ TCR \times (T_R - T_0)\}}$$

R_0 = Resistance at 0°C

R_t = Resistance at measured temperature

T_R = Temperature resistance measured

T_0 = 0°C

2.13.1 Results and discussion

The mean resistance value was calculated for each sheet of printed substrates, and from this the overall mean was determined. The individual percentage of deviation from the overall mean was calculated to locate sensor substrates in the range of +/-1% and +/-2.5% (Table 12).

Table 12 - Mean resistance values at 0°C, standard deviations and mean tolerances' for 3 sheets of sensor substrates.

	Mean resistance at 0°C (Ω)	S.D Ω)	±1.0% of mean	±2.5% of mean	±2.51 - ±5% of mean
Sheet 1	10.44	0.59	20	31	49
Sheet 2	10.48	0.54	20	43	67
Sheet 3	10.61	0.60	22	39	56
Overall mean	10.51	0.58	Total 62	Total 113	Total 172

The resistance values were measured again at 22°C. Substrates with a resistance between 10.86Ω – 11.08Ω were selected on the basis of +/-1% tolerance and substrates with a resistance between 10.7Ω – 11.24Ω on the basis of +/-2.5% tolerance.

2.14 Metal oxide paste formulation

Two types of metal oxide pastes were formulated for coating sensor substrates. There was some debate about the effect that the grain size and purity of the metal oxide would have on the sensitivity of the sensor. To investigate this, a higher purity tin oxide with a finer grain size was used to formulate one paste and a slightly lower purity tin oxide was used to formulate the other. Both types of pastes were deposited onto sensor substrates using a doctor blading technique (described in section 2.17)

2.14.1 Method

To formulate the pastes, deionised water (2.5g), tin oxide powder (2.0g) and zinc oxide (2.0g) were added together in an agate pestle and mortar and ground continuously for 30 minutes inside a plastic bag ensuring water loss was kept to a minimum.

2.14.2 Supplier information of metal oxide powders used

Zinc oxide

Supplier - BHD Chemicals

Product number - 10298

Purity - 99.5% (AnalaR grade)

Tin (IV) oxide (lower purity)

Supplier - Sigma Aldrich

Product number -244651

Purity - 99.9%

Tin (IV) oxide (higher purity)

Supplier - Alpha

Product/lot number – S20495

Purity - 99.996%

2.14.3 Results and discussion

Samples taken from the two types of metal oxide pastes were taken for optical analysis. An environmental scanning electron microscope (ESEM) was used to assess the average particle size before and after grinding. This particular ESEM (Philips XL30-Oxford Instruments Link ISIS EDX system) used an energy dispersive x-ray technique (EDX), and the following images were acquired at UWE by Dr Dave Patton. Twenty measurements were taken at each paste phase to obtain the mean value (see tables 13 and 14).

Table 13 – Particle size measurements for 99.996% tin oxide and 99.5 % zinc oxide before and after grinding

Paste phase	**Mean particle size (µm)**	**Smallest (µm)**	**Largest (µm)**
Before grinding	6.4	1.1	28.2
After grinding	0.9	0.2	2.2

Figure 25

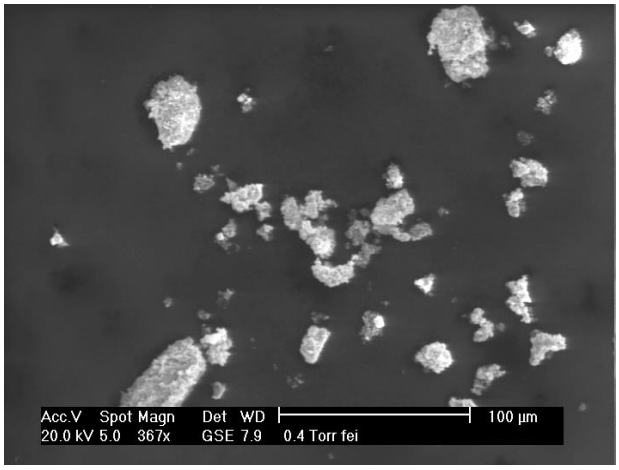

Figure 26

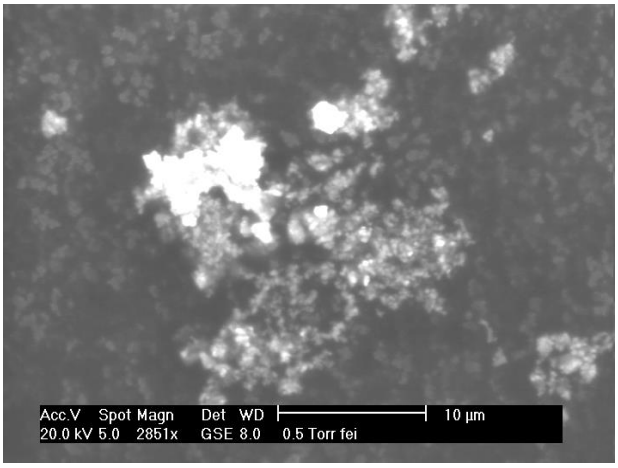

Figure 25 99.996% tin oxide and 99.5 % zinc oxide before grinding. Figure 26 99.996% tin oxide and 99.5% zinc oxide after grinding.

Table 14 – Particle size measurements for 99.9% tin oxide and 99.5 % zinc oxide before and after grinding

Paste phase	**Mean particle size (µm)**	**Smallest (µm)**	**Largest (µm)**
Before grinding	0.4	0.1	1.4
After grinding	0.9	0.3	2.0

Figure 27

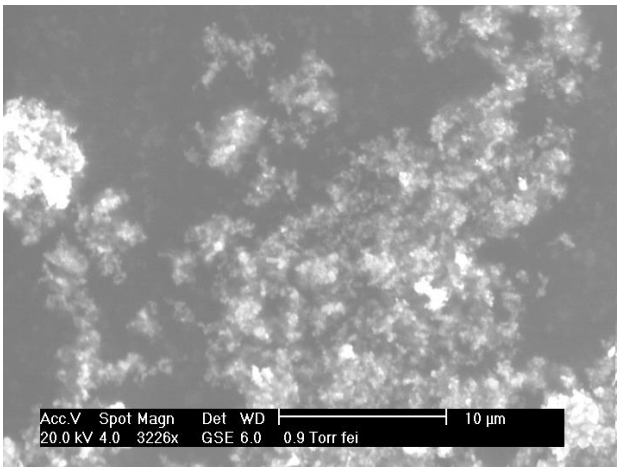

Figure 28

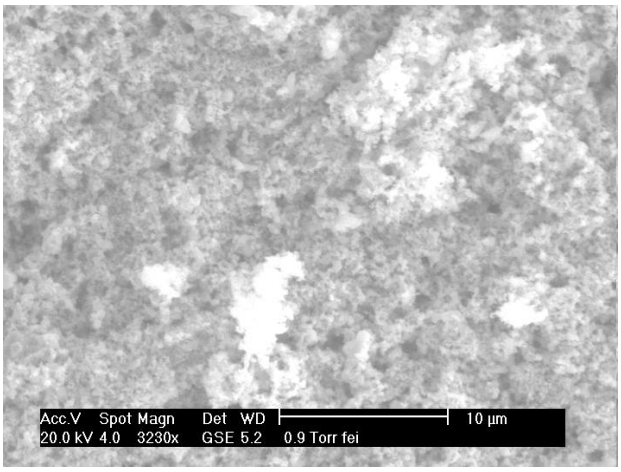

Figure 27 99.9% tin oxide and 99.5 % zinc oxide before and grinding. Figure 28 99.9% tin oxide and 99.5 % zinc oxide after grinding.

A preliminary quantitative analysis was undertaken. Further study is needed to confirm these results. Both types of metal oxide pastes look similar before grinding. After grinding, the 99.996% tin oxide based paste has much smaller particles than the 99.9% tin oxide based paste. Table 13 show that the 99.9% tin oxide based paste has particle sizes which are similar the measurements obtained before grinding, suggesting that grinding has little effect with this mixture. In contrast, the 99.996% tin oxide based mixture showed a reduction in particle size after grinding (see table 14). The mean particle size of the 99.996% and 99.9% tin oxide based

paste was 0.9µm for both mixtures. If this mean is applied for the whole of the sensors, then there would be the same sensor surface area for the 99.9% and the 99.996% tin oxide based pastes. This implies that there would be an equal surface area for volatiles to be adsorbed onto both types of paste and therefore both will give similar responses to samples and standards.

2.15 A comparison of metal oxide paste deposition methods

The method used to deposit the metal oxide paste had to ensure selective coverage of the sensor i.e. avoidance of the contact pads. The sensor was designed to be housed in a transistor can, suspended by fine wires connected to the contact pads on both sides of the sensor substrate. To enable this, it was essential that the contact pads remain un-coated.

Two methods were explored for the application of the metal oxide paste, the first being screen printing.

The benefits of screen printing metal oxide paste include;

1) Uniform thickness
2) Multiple sensors coated in one screen print
3) Assurance of paste batch consistency
4) The use of a mask would ensure that contact pads remain un coated

Potential complications of screen printing paste application

1) There was some doubt as to whether the metal oxide paste would be the right viscosity for screen printing and if not whether it would cause blockages in the screen that could not be removed. A blocked screen means that the paste will not pass through the mesh onto the sensor substrate resulting in an incomplete layer of the deposited film.
2) There was concern that the sensor substrate would stick to the screen after printing due to the inserts made to house each sensor substrate being slightly larger than the sensor substrates themselves. The inserts were made this way to allow a small amount of room for sensor substrate insertion and removal.

The second method explored for metal oxide paste application was doctor blading. Benefits of this process include;

1) Complete coverage i.e. no blockages caused by the use of a mask
2) Lower cost due to the elimination of masks
3) Relatively straight forward procedure
4) Selective coverage could be achieved through manual application

Potential complications of doctor blading paste application

1) Uneven surface
2) No assurance of paste batch consistency
3) How to make the process reproducible

2.16 Trials for screen printing a metal oxide paste

To explore this method of application, a custom built screen printing device was made. The screen printing jig was designed to house 25 sensors substrates that would sit perfectly flat in an aluminium plate and provide a smooth and flat surface for screen printing. In contrast to conventional screen printing practice, the alumina sheet was separated into individual sensor substrates before screen printing due to the delicate nature of the metal oxide paste and unavoidable damage that would be caused to the paste if substrate separation occurred after screen printing.

A mask was designed specifically for this screen printing device using the same methods described in section 2.9.1. The mask consisted of 25 rectangles that were equal in size to the area of the interdigitated electrodes.

The screen printing jig consisted of an aluminium base plate with 6 push clamps spaced evenly on each side and an aluminium substrate plate with 25 inserts for sensor substrates (see figure 29).

2.16.1 Dimensions of the custom built screen printing jig

Base plate - 335mm x 267mm x 6mm

Substrate plate - 260mm x 190mm x 6mm

Substrate Inserts – 3mm x 3.1mm x 0.635mm

To assemble the device the sensor substrates were inserted into the aluminium substrate plate that was then placed on top of the aluminium base plate. The screen printing mask was placed on top of the substrate plate and aligned with the sensor substrates and finally secured in place with 6 push down clamps.

Figure 29 - A CAD drawing of the hand screen printing bed commissioned by K Vaughan produced by Kevin Slater at Manor Farm Engineering.

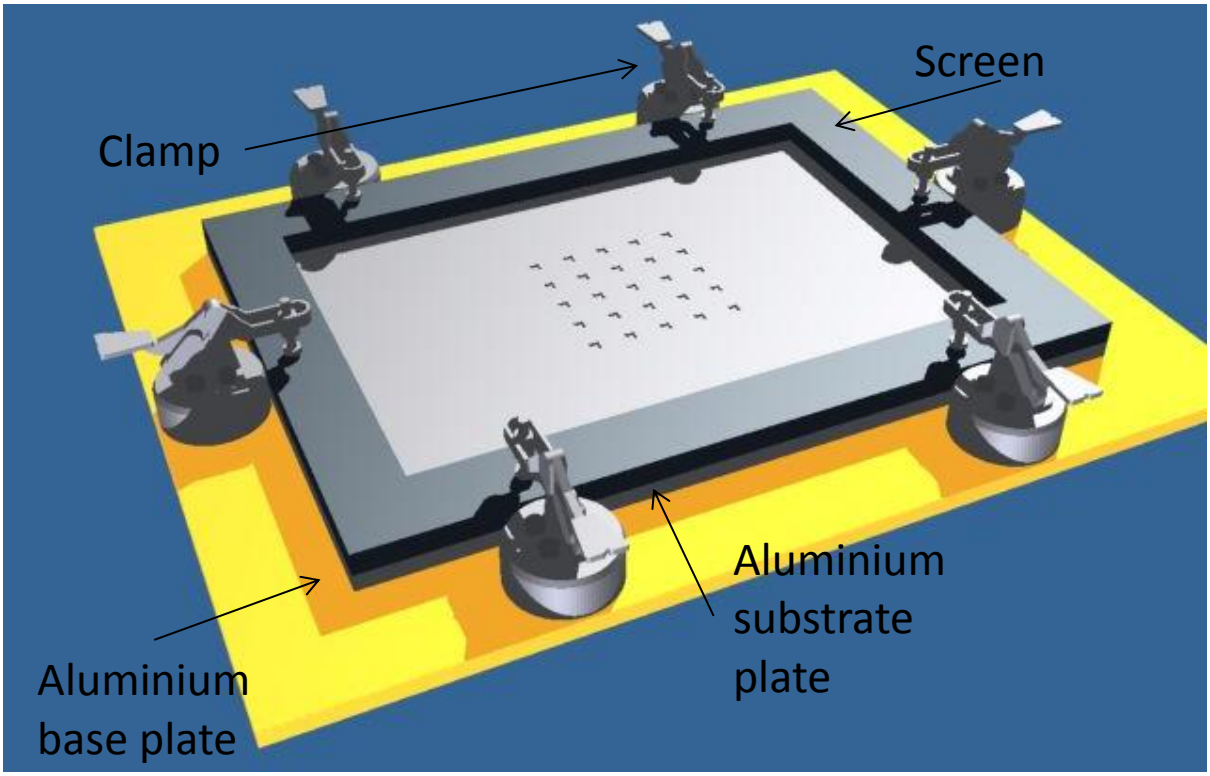

2.16.2 Results and discussion

Initial trials showed that 3 major problems were preventing the process from working. They were;

1) The substrates got stuck to the screen after the squeegee had pushed through the ink and the mask removed

2) Aligning the screen and the substrates needed to be more controlled
3) The metal oxide paste blocked the screen meaning that after 1 or two screen prints, the screen was unusable
4)

Overcoming problems 1-3

It was postulated that if a vacuum was made between the base and the substrate plates, the sensor substrates would be held firmly in place rather than sticking to the mask. Adapting the jig to facilitate a vacuum involved 3 main steps;

1) Drilling a hole through the centre of each insert
2) Adding a rubber seal between the base and substrate plate
3) Connecting a tube to the vacuum pump to be inserted through the rubber seal via a needle

2.16.3 Additions made to manual screen printing jig

To overcome mask alignment issues, locator screws were added to the jig along a vertical and a horizontal edge of the base plate (see figure 30). This enabled minor adjustments to be made to the alignment of the mask before being secured by the clamp.

Figure 30 – Locator screw addition to hand screen printing bed commissioned by K Vaughan produced by Kevin Slater at Manor Farm Engineering.

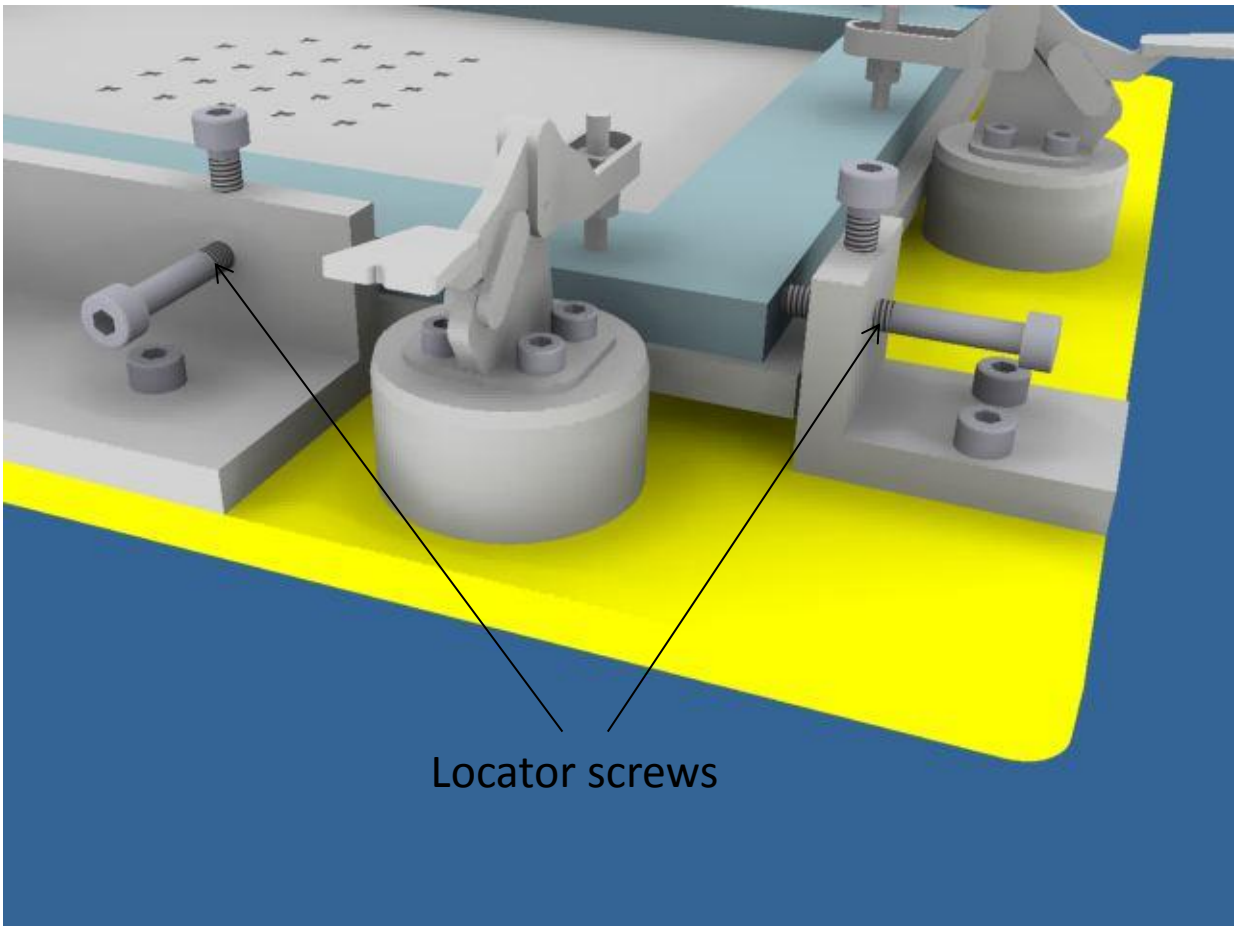

2.16.4 Summary

The addition of locator screws to the screen printing jig successfully helped to overcome alignment issues and the application of a vacuum kept the sensors in the substrate plate during the screen printing process. However, initial concerns about the viscosity of the metal oxide paste were confirmed and after the first screen print, the mask was significantly blocked and caused problems on the second screen print. When using inks specifically formulated for screen printing, a high powered water hose is usually enough to remove ink from the screen, however this alone was not enough to remove the metal oxide paste. Detergent (Decon 90, 10% in water) was added and slightly improved paste removal, but it was not enough to unblock the screen. Placing the mask in an ultrasonic water bath was also tried but had no significant effect. It was decided that this issue would be dealt with by using a new mask for each screen print. If this process could have been successful and thus commercialised, the benefits of screen printing the metal oxide paste onto the sensor substrates would far outweigh the cost of making the masks disposable. However it was not possible to surmount the problem of incomplete screen prints due to the paste not passing though the mask. This resulted in incomplete-patchy coating of sensor substrates and further attempts to develop the process were abandoned.

2.17 Doctor blading trials

Doctor blading describes the process of adding or removing wet material from a surface using a blade/spatula. The term is believed to have come from a blade that was used in conjunction with ductor rolls on letterpresses, and eventually 'ductor blade' became 'doctor blade'.

2.17.1 Method

An alumina base was made to surround individual substrates. The thickness of the base was 50µm greater than that of the sensor substrate, to give a paste thickness of 50µm.

A sheet of scored alumina with a thickness of 635µm was first split in half. A row of substrates was removed from one of the two pieces using an adjustable spanner. The row was then split in half and 1 sensor sized substrate removed from the middle (see figures 31- 33)

Figure 31 – Doctor blading step 1

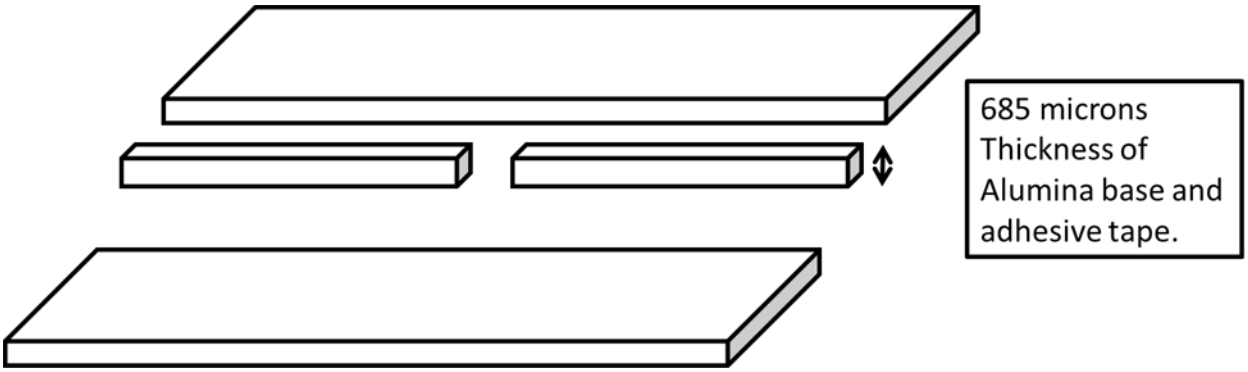

Double sided adhesive tape (Sellotape 25mm x33m supplied by Lyreco) with a thickness of 50µm (measured with a micrometer) was applied to each piece of alumina, making the total thickness of the base 685µm.

The alumina pieces were stuck down on a firm flat surface. Even pressure was applied over the surface of the base (using a roller) to ensure all alumina pieces were at the same height (see figure 32)

Figure 32 – Doctor blading step 2

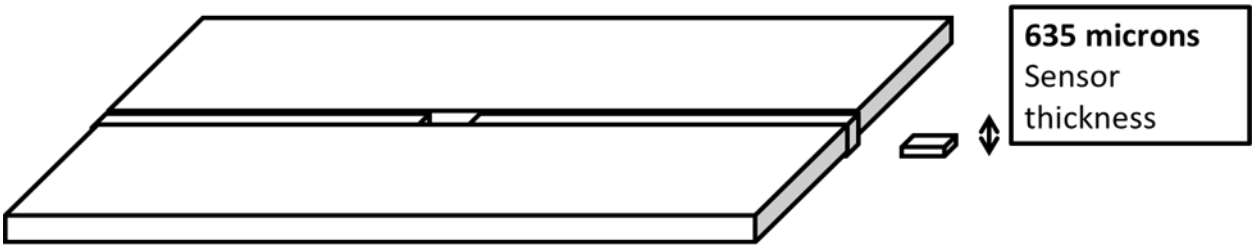

The sensor substrate was then carefully inserted into the recess at the centre of the base. A small amount of paste was applied to the blade (250µm thick piece of alumina) and deposited on the interdigitated part of the sensor. The blade edge rested on the surface of the base and was scraped vertically across the interdigitated part of the sensor (avoiding the contact pads). Excess paste was removed and the blade cleaned, before the action was repeated again horizontally (see figure 33)

Figure 33 – Doctor blading step 3

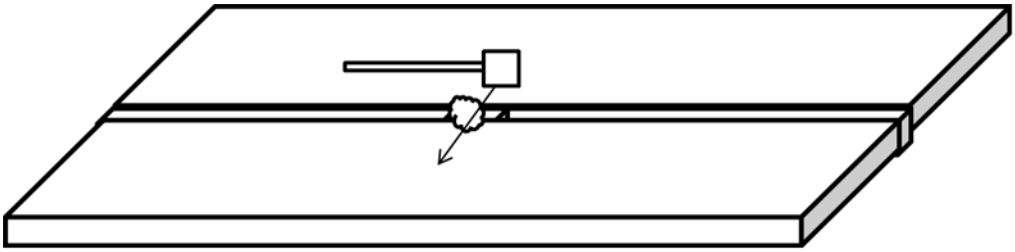

While the paste was still wet, the sensor was carefully removed and left to dry at 22°C over night. The paste was successfully deposited using this technique.

Figure 34 – Photograph of alumina bases, purpose built for doctor blading sensors

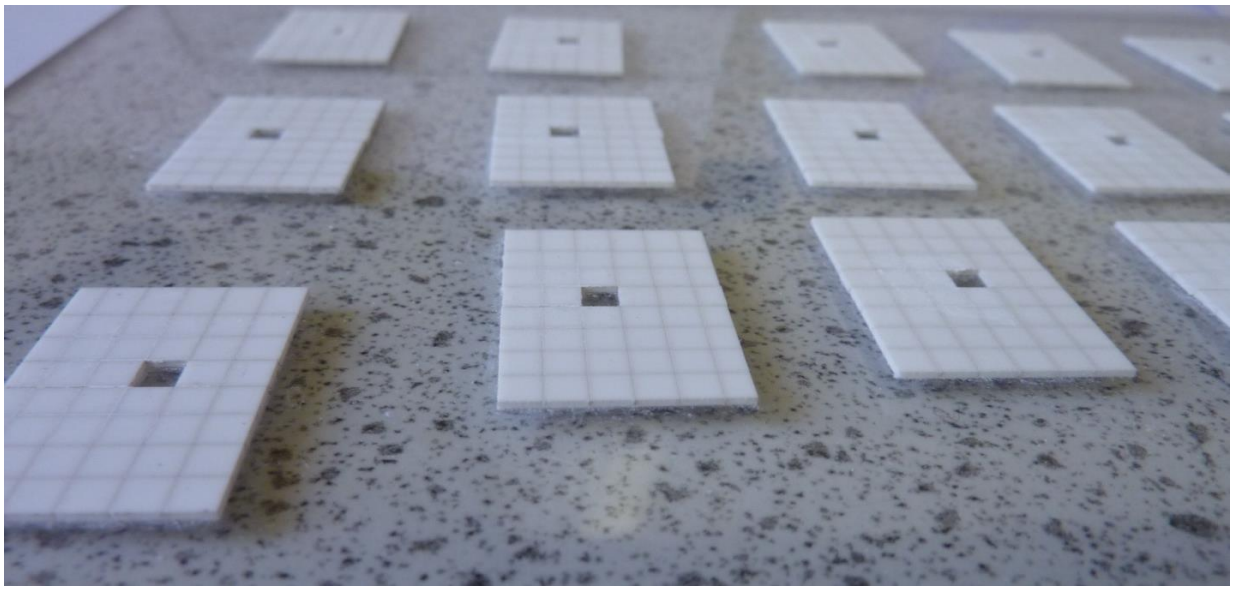

Figure 35 - Photograph of sensors coated using doctor blading method

2.17.2 Results and discussion

The doctor blading process proved successful in depositing a thin layer of the metal oxide paste onto the interdigitated electrode part of the sensor without covering the contact pads. This method was adopted to coat a selection of sensor substrates in order to assess the reproducibility of the paste thickness, its suitability for wire bonding and its overall sensing properties.

2.18 Measurements of paste thickness for doctor bladed substrates

Using a Microspectrophotometer, (MSP) the paste thicknesses of 10 sensors was measured to obtain a mean paste thickness for each sensor and an overall mean thickness and S.D. The sensors had been coated using the doctor blading technique described in section 2.17 and were individually stuck down to a slide (using double sided sticky tape) so that the edge of the substrate was facing up, giving a side on profile of the paste. Three measurements were obtained at different points along the substrate edge and recorded, the results of which can be seen in table 15.

2.18.1 Results and discussion

Table 15- Paste thickness measurements recorded for sensors 1 – 10

	Measurement 1(µm)	Measurement 2 (µm)	Measurement 3(µm)	Mean µm	Overall mean (µm)	S.D. (µm)
Sensor 1	55.8	67.0	48.4	57.0	64.2	8.6
Sensor 2	65.1	68.8	63.2	65.7		
Sensor 3	76.2	61.4	61.4	66.3		
Sensor 4	53.9	78.2	74.4	68.8		
Sensor 5	61.5	46.5	72.5	60.2		
Sensor 6	89.3	74.4	74.4	79.4		
Sensor 7	57.7	52.1	55.8	55.2		
Sensor 8	52.1	59.5	42.8	51.5		
Sensor 9	78.2	61.4	53.9	64.5		
Sensor 10	80.0	61.4	79.9	73.8		

The doctor blading method showed good reproducibility in terms of paste thickness with an overall mean (from 30 measurements) of 64.2µm and a S.D. of 8.6µm.

2.19 Electrical characteristics of sensors – Platinum heater resistance measurements

To investigate the effect of temperature change on the resistance of the sensors platinum heater, 26 sensors were heated up in an oven at 1°C temperature increments between 21°C

and 120°C. The resistance of the heater element and temperature of the oven was measured and recorded at each interval.

2.19.1 Method

Each transistor can (containing a sensor) was soldered onto a pin header that slotted into a pin header socket. The socket was soldered to a bread board with long lengths of wire attached, connecting to the platinum heater. To keep the breadboard flat whilst in the oven, 4 holes were drilled into each of the corners. This enabled a metal wire to be threaded through the holes in the breadboard and looped round the grate of the oven floor to secure the sensor unit in place. A thermocouple (type K thermocouple) was used to monitor the temperature of the oven and was secured within a few millimetres of the sensor surface.

Each sensor unit was placed into the oven (LTE Scientific Ltd OP60) and heated to 120°C. The 2 wires that connected to the platinum heater were fed outside the oven door and the resistance was measured using a multimeter (Rapid 328DMM).

2.19.2 Results

Figures 36-39 show representative plots of resistance against temperature taken every °C. The black line in each plot shows the line of best fit and the linear equation is shown on the graph. This equation can be used to calculate resistance values of the heater at a given temperature, assuming the linear relationship holds between the temperature and resistance at that temperature. The '+' value in the equation represents the resistance at 0°C ($R_{0°C}$). This can be found by tracing the line of best fit back to where it intercepts the Y axis.

Figure 36- Graph of temperature against resistance for sensor 3

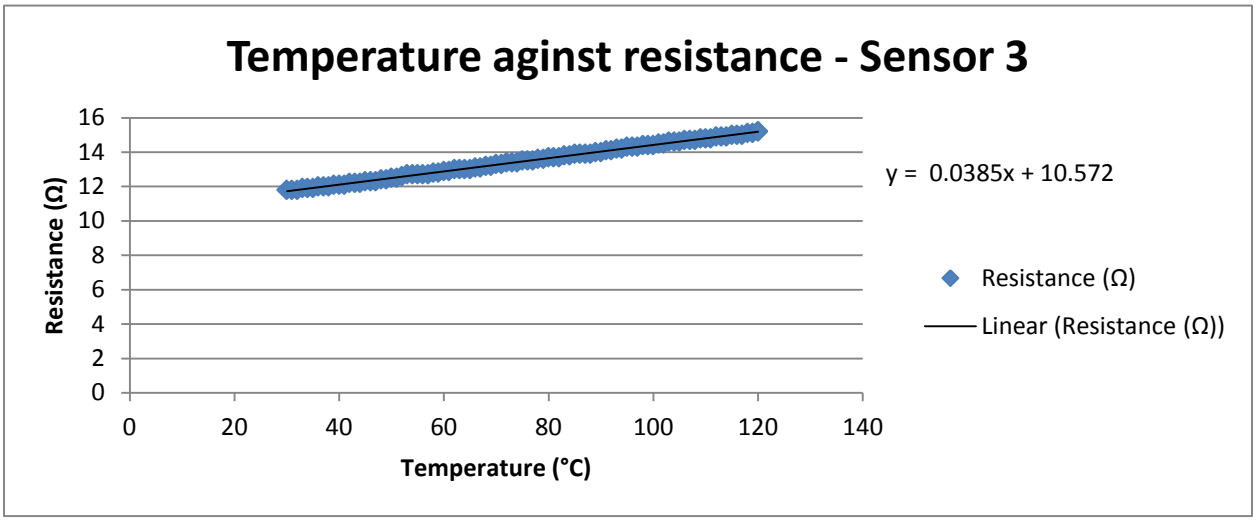

Figure 37 - Graph of temperature against resistance for sensor 10

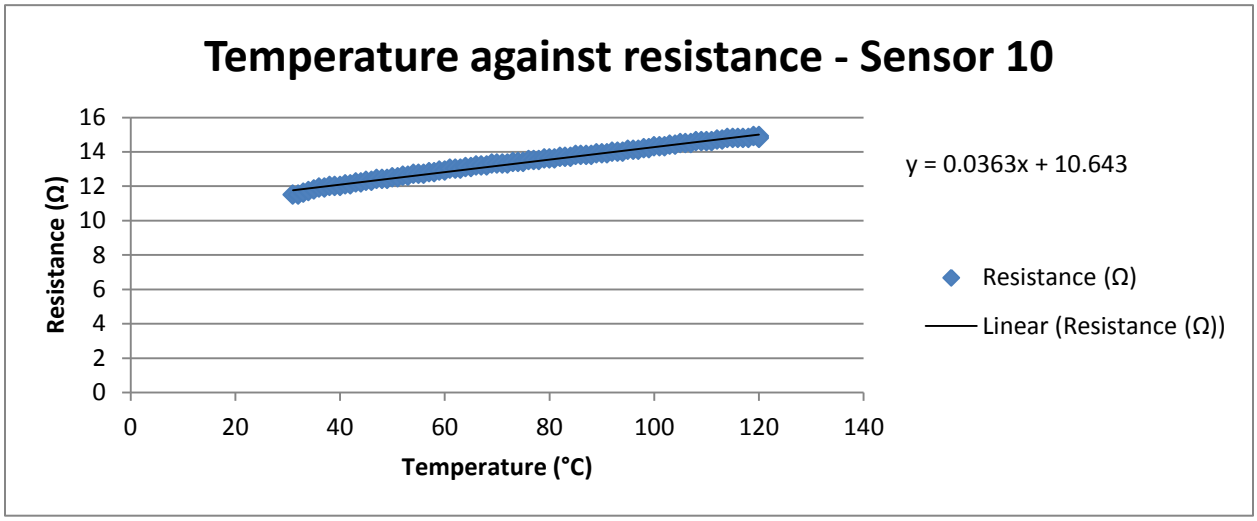

Figure 38- Graph of temperature against resistance for sensor 19

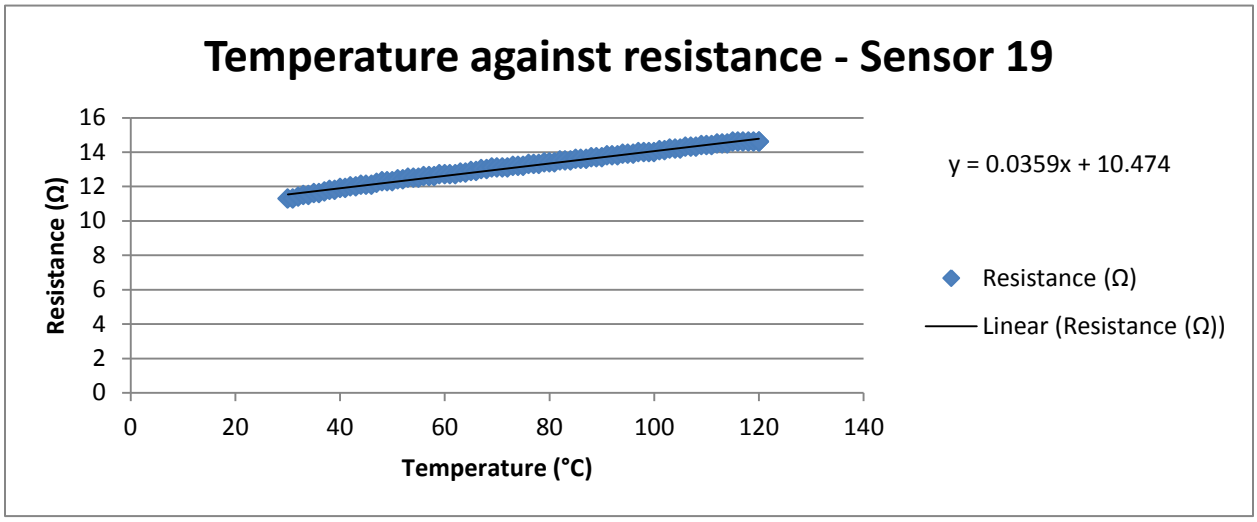

Figure39- Graph of temperature against resistance for sensor 23

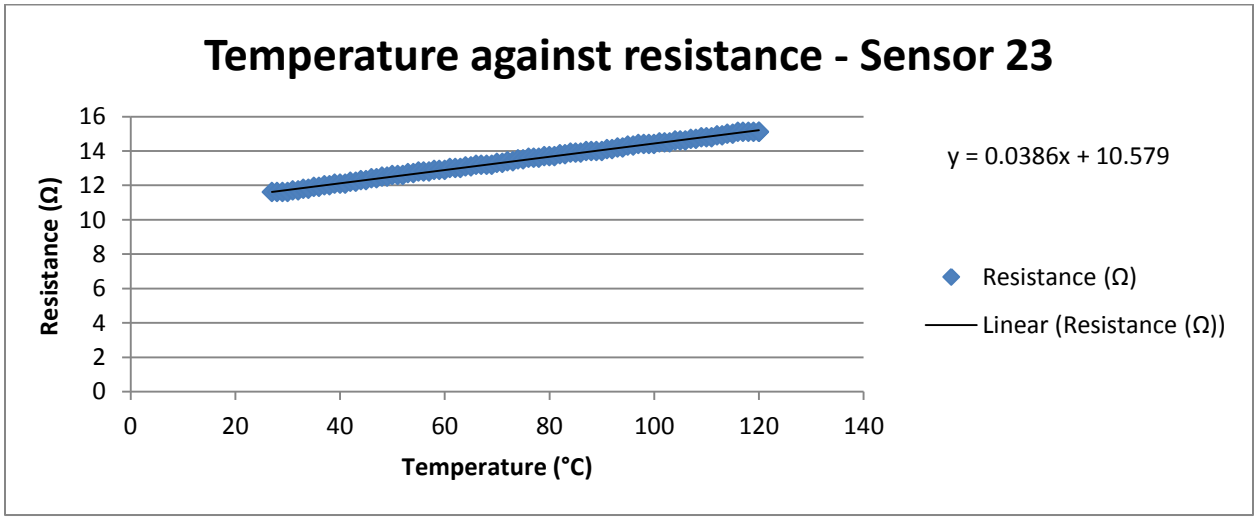

2.20 Calculations required for gas analysis equipment

The linear equations obtained from measuring the heater resistances of the 26 sensor above, were used to calculate the resistance at 0°C ($R_{0°C}$), resistance at 100°C ($R_{100°C}$) and the temperature coefficient of resistance (TCR). These values are required for precision gas analysis

equipment which has the capability to use these parameters to set the sensor at 450°C either by the software control or manually by electronic means. The former is the case for the OdoReader system, a collaborative device built for analysing volatiles in urine and stool.

Table 16 shows the R_0°C (as shown in the linear equation for each plot in figures 35-38), resistance at 100°C ($R_{100°C}$) and the TCR values for sensors 1-26.

The $R_{100°C}$ was calculated using the gradient (y value) of the linear equation and the R_0°C (see equation 1 below) and the TCR calculated using the $R_{100°C}$ and R_0°C (see equation 2 below, equation reference: Hernández, C.A. and Wilson, J.D. (2009) *Physics Laboratory Experiments* [online]. 7th ed. Usa: Cengage Learning. [Accessed 22 July 2013].

2.20.1 Equations for calculating TCR and $R_{100°C}$

1. $R_{100°C} = (y \times 100) + R_0°C$

2. $$TCR = \frac{R_{100°C} - R_{0°C}}{R_{0°C} \times 100°C}$$

Table 16 $R_{0°C}$, $R_{100°C}$ and TCR value for sensors values for sensors 1-26

Sensor	$R_{0°C}$ (µm)	$R_{100°C}$ (µm)	TCR (Ω/°C)
1	10.9	14.6	0.00342
2	10.7	14.5	0.00358
3	10.6	14.4	0.00364
4	10.6	14.5	0.00360
5	10.5	14.1	0.00335
6	11.0	14.7	0.00333
7	10.9	14.6	0.00343
8	11.2	15.0	0.00345
9	10.8	14.5	0.00344
10	10.6	14.3	0.00341
11	11.0	14.9	0.00348
12	11.2	15.1	0.00346
13	10.8	14.6	0.00354
14	11.1	14.8	0.00330
15	11.0	14.6	0.00333
16	11.2	14.9	0.00336
17	11.1	14.8	0.00340
18	11.0	14.8	0.00336
19	10.5	14.1	0.00343
20	10.9	14.6	0.00341
21	10.7	14.4	0.00352
22	10.5	14.3	0.00364
23	10.6	14.4	0.00365
24	10.8	14.7	0.00353
25	10.9	14.7	0.00343
26	11.0	14.9	0.00355

Table 17- Mean $R_{0°C}$, $R_{100°C}$ and TCR value for sensors 1-26 along with the standard deviation and maximum and minimum values recorded.

	$R_{0°C}$ (Ω)	$R_{100°C}$ (Ω)	TCR(Ω/°C)
Mean	10.8	14.6	0.00346
S.D.	0.23	0.26	0.00010
Maximum value	11.2	15.1	0.00365
Minimum value	10.5	14.1	0.00330

2.20.2 Results and discussion

A summary of the results in table 17 show that the calculated mean resistance for the 26 sensors at 0°C was 10.8Ω with a S.D. of 0.23Ω. The mean calculated resistance at 100°C was 14.6Ω with a S.D. of 0.26Ω. These results show that there is little variation of the heater resistance between the sensors tested here.

Chapter 3 – Assembling the sensor

3.1. Joining the sensors to transistor cans

Once the sensors substrates had been coated with the metal oxide paste, post wire bonding techniques were required in order to join the sensors to transistor cans. This would enable a simple installation of the sensor in the OdoReader device.

3.2 Parallel gap resistance welding

The application of electrical current and mechanical pressure was used to form resistance welds between metals. The optimum parameters for resistance welding of the coated sensors were determined (e.g. by decreasing the pressure and increasing the current) and set up. This work was carried out by personnel at The Welding Institute (details below).

Supplier of service – The Welding Institute (TWI), personnel – Dr Helen Goddin, machine model- Miyachi Electrode Tip Resistance Welder, electrode tool – Miyachi.

3.2.1 Selection of metal wire

Three types of metal wire were used; gold, platinum and nickel to determine the quality of bonding to the sensor substrates. These three metals were selected for their high temperature melting points and their ability to withstand oxidation in air. Nickel was of particular interest to see whether it would give comparative weld strengths to platinum and gold wire, because of its relatively low cost. Out of the 3 metals platinum was the favoured choice due to its much

higher melting point and the possibility that that the temperature of the sensor could be increased if it was found to be necessary.

3.2.2 Transistor can details

Supplier of transistor can - Eltek semi conductors Ltd, product details- SL.01.379.018. Schott cans (T039 headers), supplier address- Nelson Road Industrial Estate, Dartmouth, Devon, TQ6 9LA.

3.2.3 Initial tests

The wire was first welded to the 2 contact pads on the platinum side of the sensor and then to the 2 pads on the interdigitated side. The loose end of the gold wire was then welded to one of the 4 pins on a transistor can suspending the sensor in the centre of the transistor can (see figure 40).

Figure 40 – Photograph of an uncoated sensor welded to a transistor can

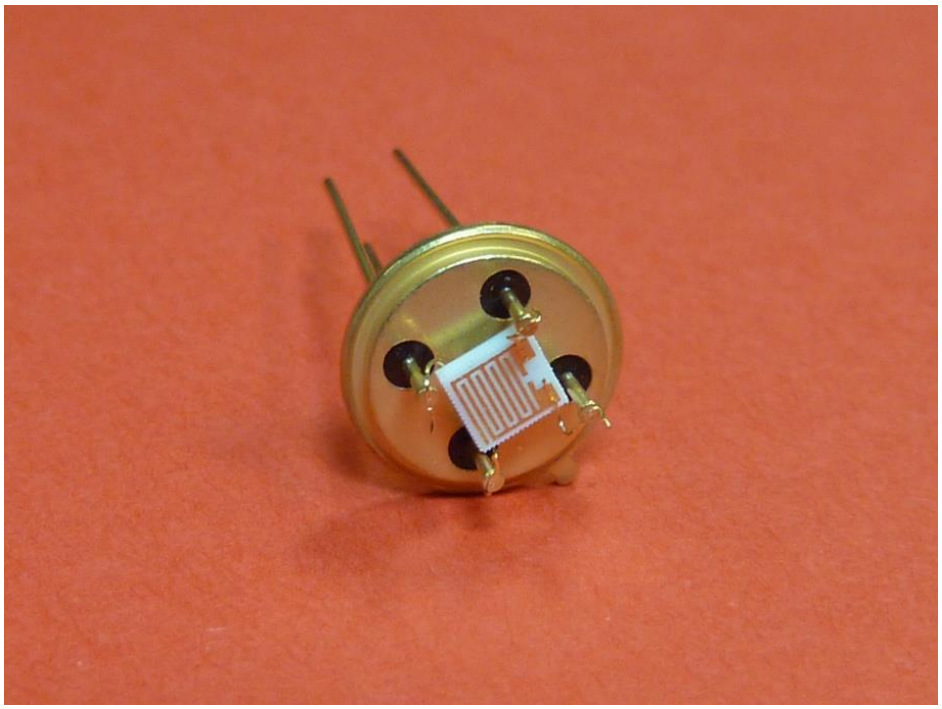

There was some scepticism as to how well the platinum wire would bond to the gold and platinum ink (private communication with Dr Helen Goddin at The Welding Institute, Cambridge). However the advice given was that gold wire would form strong bonds to gold ink. The sensors were divided into three sets, each with a different configuration for some resistance welding experiments (see table 18).

Table 18– Sensor sets with different configurations for resistance welding experiments

Set	Side A	Side B
1	Interdigitated gold electrodes	Platinum heater with platinum contact pads
2	Interdigitated gold electrodes	Platinum heater with gold contact pads printed over existing platinum contact pads
3	Interdigitated gold electrodes with extra layer of gold printed over existing contact pads	Platinum heater with gold pads printed over existing platinum contact pads

Sensors in set 1 consisted of interdigitated gold electrodes printed on one side of the alumina substrate and a platinum heater element printed on the opposite side. This configuration would demonstrate the strength of all the welds to the sensors without any extra expensive layers having to be applied to the sensor substrates.

Sensors in set 2 consisted of interdigitated gold electrodes printed on one side of the alumina substrate and a platinum heater element on the opposite side with gold contact pads printed over the existing platinum pads. If platinum wire did not bond well to platinum ink, this configuration would allow platinum wire to be bonded to gold contact pads on both sides.

Sensors in set 3 consisted of interdigitated gold electrodes printed on one side of the alumina substrate with an extra layer of gold applied to the existing gold contact pads to double the thickness and a platinum heater element on the opposite side with gold contact pads printed over the existing platinum pads. Doubling the thickness of the gold was recommended (private communication with John Whitmarsh at ESL Ltd) to increase the bond strength of the gold wire to the gold contact pads should we find the weld strengths inadequate with a single gold layer.

3.2.4 Pull tests

A qualitative assessment was undertaken to determine the strength of the resistance welds, the wires were pulled (by hand) in the direction that the welds had been formed i.e. to the side of the substrate.

The following criteria were used to assess the resistance welds;

Not good – Wires were removed from the substrate/transistor can after being pulled with little/no force

Poor – Wires were removed from the substrate/transistor can after being pulled with a small amount of force

Good – Wires were removed from the substrate/transistor can after being pulled with significant force

Very good – Wires stayed attached to the substrate/transistor can, after being pulled with significant force.

3.2.5 Results and discussion

Table 19 – Pull test results for resistance welds made to sensors in set 1

Set 1	Strength
Gold wire to platinum electrode	Good
Gold wire to gold electrode	Good
Platinum wire to platinum electrode	Not good
Platinum wire to gold electrode	Not good
Nickel wire to platinum electrode	Not good
Nickel wire to gold electrode	Poor

Table 20 - Pull test results for resistance welds made to sensors in set 2

Set 2	Strength
Gold wire to gold pad over platinum electrode	Very good
Gold wire to gold electrode	Very good
Platinum wire to gold pad over platinum electrode	Very good
Platinum wire to gold electrode	Not good

Table 21 - Pull test results for resistance welds made to sensors in set 3

Set 3	Strength
Gold wire to gold pad over platinum electrode	Very good
Gold wire to gold pad over gold electrode	Very good
Platinum wire to gold pad over platinum electrode	Not good
Platinum wire to gold pad over gold electrode	Not good

Table 22 - Pull test results for resistance welds made to transistor cans

Wire	Strength
Gold wire	Very good
Platinum wire	Very good
Nickel wire	Very good

Gold wire (Sigma Aldrich 99.9% trace metals basis 0.127mm wire diameter, 267812-270mg, 100cm) was chosen in combination with the sensor configuration from set 2 as the gold wire made strong welds to the gold paste. Sensors from set 3 could have also been used, however the extra layer of gold paste over the interdigitated electrode pads would increase the cost to the fabrication process when the welds made to a single layer of gold paste were of similar strengths.

3.3 Sensor chamber designs

The transistor can was mounted to a 24 pin header (Farnell, product code 1136776). A 10mm hole was drilled in the base of the pin header to prevent it from heating up and giving off volatiles (see figure 41). The sensor reaches temperatures of at least 450°C, and is designed to be in operation 24 hours a day. To ensure that heat from the sensor was not transferred to the pin header socket a sheet of alumina (250µm thick) was inserted between the two parts. Each of the 4 transistor cans pins were soldered (60/40 tin-lead multicore solder,0.71mm, RS components- order code 555-235) to one of the contacts on the pin header. A brass bar with a hole drilled in the centre was used to stabilise a thin metal tube that guides the column to the coated sensor surface.

Figure 41 - Sensor unit

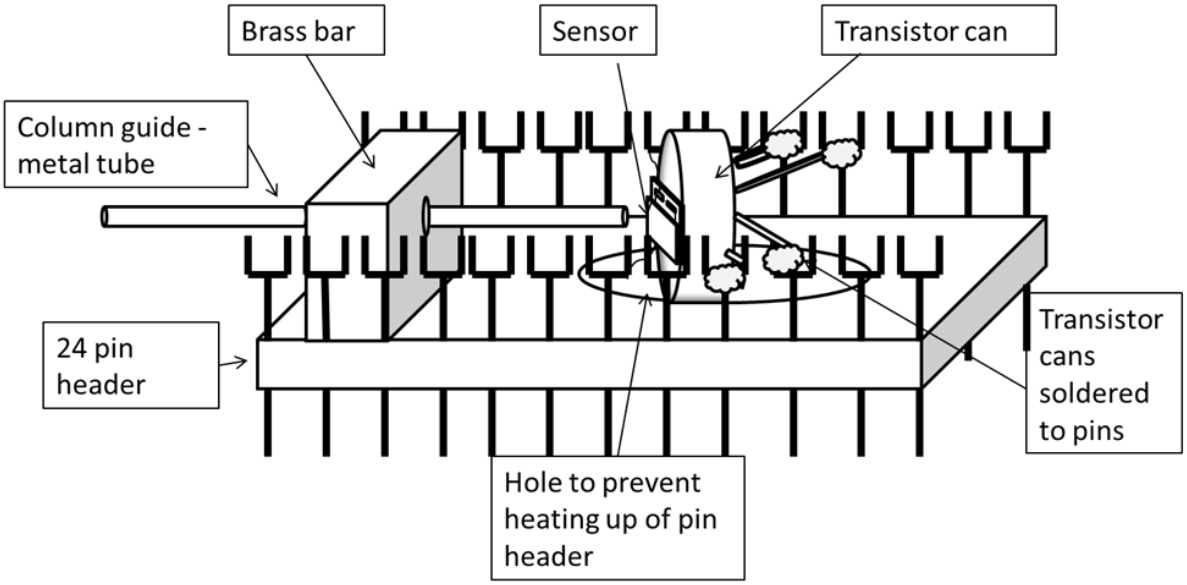

Figure 42 shows the mark 1 sensor chamber. This consisted of the transistor can soldered to a pin header, fixed into a metal box shown on the right hand side of the photograph. The outlet from the column went through a needle guide so that the volatiles from the column blew onto the sensor. There was an inlet for pure air and an outlet to purge the chamber.

Figure 42 – Mark 1 sensor chamber with column

Mark 2 sensor chamber

The mark 2 sensor chamber was built of stainless steel, to minimise volatiles sticking to the chamber surface. The chamber was a much smaller volume than the mark 1, enabling faster purging. See figures 43 and 44 below for sensor chamber design.

Figure 43- Plan view of sensor chamber

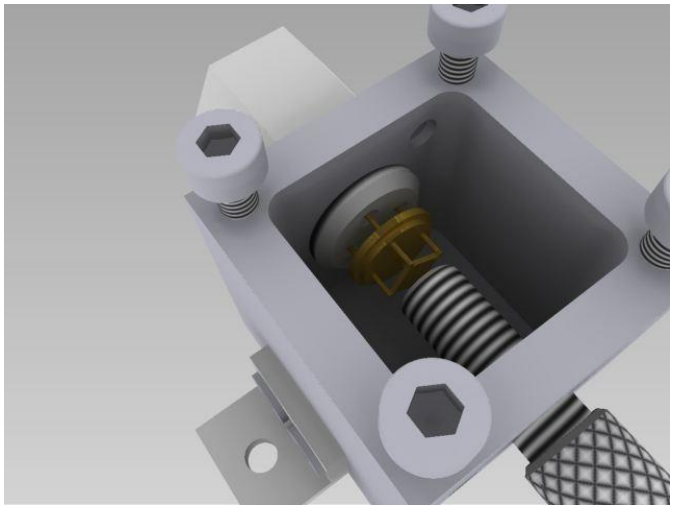

Figure 44- Side view of sensor chamber

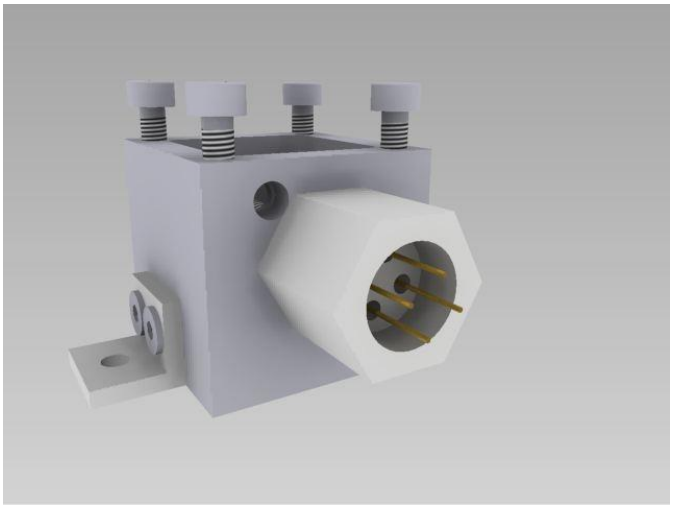

3.4 Testing the electrical resistance of coated sensors in OdoReader

To assess the reproducibility of the sensor, the interdigitated electrode resistances of 25 sensors were measured. Each sensor unit was inserted into an IC socket (Farnell - 2227MC-24-06-F1 – socket, DIL, tube/20, 24 way) inside the OdoReader system. The temperature of the sensor was set to approximately 450°C and the baseline was left to stabilise for 60 minutes. The resistance was recorded for a further 20 minutes and a mean resistance value was obtained for this period.

After 100 minutes, 3 x 2cm^3 ethanol (50ppm) injections were made into the GC. The size of the peak was measured and a percentage of change in resistance (sensitivity) was calculated using the equation below.

(Change in resistance / resistance value at the middle of the peak) x 100

3.4.1 Results and discussion

A mean sensitivity was then calculated for each sensor. Table 23 shows the data for these trials.

Table 23 Electrical resistance statistics of 25 sensors

Sensor	Mean resistance (Ω)	Maximum (Ω)	Minimum (Ω)	S.D.	Injection 1(%)	Injection 2 (%)	Injection 3 (%)	Mean (%)
2	176081	181563	171386	2926	325	276	297	299
3	210475	211118	209154	329	213	267	219	233
4	167427	170205	165157	1443	294	291	260	282
5	72357	73664	70189	982	212	234	232	226
6	105121	107475	102686	1332	188	224	192	201
7	114591	116246	113345	745	201	210	257	223
8	138331	139997	137237	749	278	250	263	264
9	77476	82948	72777	2831	140	166	166	157
10	61067	62234	60243	551	132	165	186	161
11	98438	100234	96700	1002	187	234	250	224
12	109910	112572	106756	1707	190	204	229	208
14	162243	168805	154701	4003	210	270	264	248
15	83615	88969	79758	2483	129	146	144	140
16	99190	102010	97330	1289	154	189	161	168
18	98222	99906	96700	829	157	158	212	176
19	58432	58723	58092	128	197	203	201	200
20	118266	120935	115844	1185	223	242	252	239
21	116704	119529	114257	1373	187	172	187	182
22	88089	89346	86660	757	166	192	192	183
23	117542	118420	116784	416	194	268	218	227
24	121618	122077	121219	187	276	329	327	311
25	115168	119389	11679	2094	177	177	173	176
26	165201	166966	162718	978	223	249	274	249

Table 24 Mean values and S.D. of 25 sensors

Mean baseline resistance (Ω)	S.D. (Ω)	Mean sensitivity (%)	S.D. (%)
116629	38664	216	43

Although the baseline resistance varied there was much less variation in the percentage change of resistance. For example, the lowest baseline was recorded for sensor 19 at 58432Ω with a mean response to ethanol of 200%. The highest baseline recorded was for sensor 3 at 210475Ω with a mean sensor response to ethanol of 233%. This shows promise for the usability of sensor with large variation in baseline resistance.

3.5 Retention time study of the OdoReader system

A key component of OdoReader is a chromatography column which enables the separation of complex mixtures (analyes) from biological samples such as urine and stool. Analytes travel through the column at a rate primarily determined by their physical properties and the temperature and composition of the column. The various analytes travel through the column at different rates, exit the column (elute) and enter the heated detector. An electronic signal is generated upon interaction of the analyte with the detector. The size of the signal is recorded by a data system and is plotted against elapsed time to produce a chromatogram.

These types of samples could potentially cause a shift in retention times (the time it takes for a compound to elute from the column). This time shift would cause difficulties in using OdoReader as a diagnostic device.

3.5.1 Retention time study of sensor over 152 days

An evaluation of this potential shift was undertaken by multiple injections of urine samples over 152 days interspersed with an ethanol standard. Three injections were made on each day and a mean retention time was obtained for each day. From this an overall mean retention time and S.D. was calculated.

Table 25 Retention times of ethanol over 152 days

Day	Retention time ethanol (minutes)
1	1.28
41	1.23
62	1.31
68	1.32
74	1.31
124	1.29
145	1.31
146	1.34
152	1.37
Mean	1.31
S.D.	0.04

Very small variations were observed over the 152 day period. The cause of this variation is most likely due to user error when injecting the sample, which could be eliminated with an auto sampling mechanism. These results suggest that retention times can be relied upon to identify certain volatiles in biological samples.

3.5.2 Retention time study of newly installed sensors

Twenty five sensors were newly installed into a different OdoReader system, left for 60 minutes to stabilise and then subjected to 3 ethanol injections. Table 26 shows the mean retention time for each sensor and an overall mean and S.D.

Table 26 retention time to ethanol of 26 sensors

Sensor	Mean (minutes)	Overall mean (minutes)	S.D.
2	0.30	0.30	0.007
3	0.30		
4	0.32		
5	0.30		
6	0.30		
7	0.31		
8	0.31		
9	0.31		
10	0.30		
11	0.31		
12	0.31		
14	0.32		
15	0.30		
16	0.30		
18	0.31		
19	0.30		
20	0.30		
21	0.30		
22	0.30		
23	0.30		
24	0.30		
25	0.30		
26	0.30		

The table shows little variation between sensors with an overall mean of 0.3 minutes and S.D 0.007 minutes. It can also be observed that compared to the retention time study of the sensor

over 152 days (see table25) the retention time of ethanol in these tests is approx. 1 second earlier. This time difference is most likely due to the fact that two different systems were used in these tests. The operation programmes set for each system were slightly different i.e. carrier gas pressure. Also one would expect each OdoReader system to work differently. It is important to perform calibration tests on a regular basis with GC analysis so that these differences can be noted and factored in when samples are compared across different OdoReader systems.

3.6 Conclusion

The following bullet points are a summary of the work undertaken on the design and fabrication of sensors for OdoReader.

- Investigation into different sensor substrate fabrication techniques
- Selection of screen printing process for this work
- Successful design of 3 sensor substrates categorised as type A and type B
- Type A sensor substrates showed they were not suitable for further development
- Type B sensor substrates satisfied project requirements
- Screen printing explored as a possible deposition method for metal oxide coating
- Doctor blading explored as another possible deposition method for metal oxide coating
- Selection of doctor blading deposition method
- Testing of heater resistance showed good reproducibility
- Sensors have been installed in 3 OdoReader systems at the BRI and the heaters have been running successfully for over 6 months without failure
- Sensors are responding well to standards and stool samples over a 6 month period as part of the Wellcome funded project on diarrhoea diagnostics
- Retention time study confirms that sensors can be relied upon to give consistent results even when exposed to biological samples

Chapter 4 - Analysis of volatiles from urine for potential medical diagnostic devices

4.1 Introduction to urine analysis

The sensor described in this thesis was made for the Wellcome Trust project for diarrhoea diagnosis, but their use has been extended here for the diagnosis of UTIs.

Urine analysis is the oldest of all laboratory tests. Greeks from at least 500BC would examine a patient's urine as an important part of their diagnostic process.

What is a UTI?

A UTI is a common type of infection that occurs in the urinary tract. The symptoms of a UTI include;

- pain or a burning sensation during urination (dysuria)
- a frequent need to urinate
- lower abdominal pain

4.2 Current procedure for UTI diagnosis

Today urine analysis is routinely used for the diagnosis of urologic conditions such as calculia (kidney stone), urinary tract infections (UTIs) and malignancy. The diagnostic procedure consists of 3 parts; chemical testing, microscopic analysis and urine culture.

4.2.1 Dipstick analysis

The chemical test, also known as a dipstick, uses a plastic strip with a series of absorbent paper pads. Each pad is treated with a chemical that reacts with particular substances in the urine and when they come into contact with each other, the pad changes colour. The intensity of the colour increases in proportion to the amount of substance present in the urine.

The dipstick tests are inadequate, often giving false results and fail to identify the bacteria causing the infection therefore OdoReader was assessed as a potential diagnostic system.

Table 27 shows the reference ranges for urine sample assessment. The only three of relevance to UTI diagnosis are pH, leukocyte esterase and nitrite.

Table 27 - Dipstick reference ranges for urine samples from healthy patients

Specific gravity	1.010 -1.030
Colour	Straw/clear
Odour	None/mild
Dipstick	
pH	4.8 – 7.5
Protein	Trace
Glucose	Trace
Ketones	None
Haemoglobin	None
BIlirubin	None
Urobilinogen	None
Leukocyte esterase	Negative
Nitrite	Negative

4.2.2 Microscopic analysis of sediment

Following the dipstick examination, urine may be sent for microscopic analysis. A sample of well mixed urine is centrifuged in a test tube to produce a concentration of sediment (cellular matter) at the bottom of the tube which is then examined under a microscope. First, the sediment is examined through the microscope under low-power to identify casts, crystals, squamous (flat) cells, and other large objects.

Examination is then performed through the microscope at high power to further identify any cells, bacteria and clumps of cells or debris called casts.

4.2.3 Urine culture

Urine is normally sterile, so the presence of bacteria in urine is indicative of a UTI. If a dipstick indicates bacteria in the urine, or the patient is experiencing symptoms associated with UTIs, clinicians will often send the urine for culture to ascertain the species. Once the species is known the right antibiotic can be prescribed.

With a urine culture, a small sample of urine is placed on one or more agar plates (a thin layer of a nutrient media) and incubated at 37°C. Any microorganisms that are present in the urine sample grow over the next 24 to 48 hours as small circular colonies. The size, shape, and colour of these colonies help to identify which bacteria are present, and the number of colonies indicates the quantity of bacteria originally present in the urine sample. The plates are then observed for colonies, the total number counted and the types assessed. Sometimes, more than one type of bacteria will be present. If there is no or little growth on the agar after 24 to

48 hours of incubation, the urine culture is considered negative for pathogens and the culture is considered complete. Once the causing bacteria(s) has been identified the correct antibiotic can be prescribed to the patient.

4.3 The importance of these tests

Urinary tract infections (UTI) are remarkably common in women. Some 20% of women in the age range 20-65 years suffer at least one attack per year, 50% develop a UTI within their life time [45].

Urine cultures remains the reference standard for UTI diagnosis, however the amount of time required for detection of bacteria growth, results in delayed or inappropriate treatment. Rapid urine tests (such as the dipstick method) do not identify specific organisms and therefore can't be used to replace urine culture methods.

4.4 Analysis of volatiles from urine

There have been limited studies on the analysis of volatiles from urine to aid disease diagnosis. One study identified formaldehyde concentrations in the headspace of urine from patients with both bladder and prostate cancer [46]. This work was targeted at the one compound rather than the full range of VOCs present. Another study looked at the number of VOCs present in the urinary headspace from patients with a range of metabolic disorders [47]. GC analysis of urinary

headspace has been developed for the rapid screening and diagnosis of fish odour syndrome (trimethylaminuria) [48].

The impressive ability of dog olfactory senses has been used for the detection of bladder cancer in urine. An early study involving canines used 6 different dogs each trained using urine from patients with bladder cancer and with urine from healthy individuals or those suffering from another disease [49]. The dogs were able to pick out those samples that came from bladder cancer patients with a mean success rate of 41% compared to 14% expected by chance alone, suggesting that tumour related volatiles are present in urine, giving it a characteristic odour.

4.5 Volatile analysis of inoculated urine samples using OdoReader

The aim of this pilot study was to assess the potential for bacterial identification and UTI diagnosis through volatile analysis. There is evidence that electronic noses can detect UTIs, however the published results have not been entirely successful and have failed to identify the bacteria species responsible for causing the UTI. The sensor developed here was used in combination with a GC column (OdoReader) to assess urine inoculated with known bacteria.

4.5.1 Sensor calibration

In order to assess the sensitivity of the sensor used for these tests, a $2cm^3$ sample of 50ppm ethanol/methanol was injected into the GC column at the start of each day of experiments. This was done over a period of 152 days, the results of which can be seen in table 28.

Table 28 - Sensor response to ethanol/methanol over a 152 day test period.

Day	Methanol % response	Ethanol % response
1	72	375
41	36	161
62	163	895
68	299	1113
74	384	1342
124	278	693
145	239	583
146	177	426
152	247	708

The table shows that the sensors percentage response to ethanol was around 250% between day 1 and day 40, 1116% between day 60 and 80 and 603% between day 124 and 152. This change in sensitivity over the 152 day test period could be due in part to the sensor being newly installed in the OdoReader system. Metal oxide sensors characteristically require a conditioning period (usually in the excess of 30 days) where they are kept in air at operating temperature for 24 hours a day. Time constraints did not allow for this and although the sensor was kept heated during the 152 day period, it was also subjected to biological samples which could be responsible for causing variation in the sensors response to ethanol and methanol. The graph shows that there is some correlation between ethanol and methanol responses.

4.5.2 Method

Urine taken from 10 healthy volunteers was filtered to produce a batch of sterile stock urine that was then frozen and stored (-18°C). Five of the most common UTI causing bacteria had been utilised to inoculate the stock urine at low bacterial concentrations. The 5 bacteria chosen for these experiments were; *K. pneumoniae, S. saprophyticus, P. aeruginosa, E. faecalis and P.*

mirabilis. Volatile analysis of the inoculated urine was assessed at hourly intervals over a six hour period, the first sample being taken at time zero. A bacterial count and optical density measurement was also undertaken at the same time as the volatile analysis.

A control of filtered urine with no added bacteria was run to serve as a comparison between the volatile traces of an uninfected urine and inoculated urine.

4.5.3 Obtaining the samples

The chosen strain of bacteria was added to 10ml of filtered urine and left to grow overnight in an incubator at 37°C. The following morning 500µl of the overnight culture was added to 50ml of filtered human urine. The tests began at time zero where a 3ml sample was taken for volatile analysis, a 1ml sample for an optical density reading and a 10µl sample for plating. Once the samples had been taken, the inoculated urine was placed in an orbital shaker at 37°C to allow the bacteria to grow for 1 hour before this sample selection was repeated.

4.5.4 Method for volatile analysis

At each hourly interval, a 3ml sample of inoculated urine was pipetted into a headspace sampling vial. The vial was placed into a water bath at 60°C for 10 minutes. The vial was then removed and $2cm^3$ of the headspace gases were extracted using a hypodermic needle and a glass syringe. The headspace gases were then injected into the GC column. The initial GC oven temperature was 40^oC with a 6 minute hold at this temperature, then the temperature was ramped up at a rate of 5^oC/min to 100^oC with a 22 minute hold at this temperature to give a total run time of 42 minutes. The carrier gas (air) pressure was 35 psi.

To ensure that the glass syringe did not absorb any volatiles from the previous sample, it was placed in an oven for 60 minutes at 200°C between each use.

4.5.5 A visual assessment of the chromatogram results

A chromatogram was generated by GCDetector ANN/OdoReader for each hourly interval with all 5 bacteria. The chromatogram mapped the sensors response to the presence of volatiles over a 42 minute period. It is possible to observe differences between volatile trace patterns by looking at the chromatograms. Figure 45 shows a screen shot of the control which was used to compare samples infected with known bacteria.

Figures 46-50 show representative screen shots of a chromatogram for all 5 bacteria at roughly 10^5 cfus/ml, during the first five minutes of the 42 minute run.

Figure 45 - Chromatogram showing the volatile trace pattern with time for the control sample Minutes 0-5 expanded

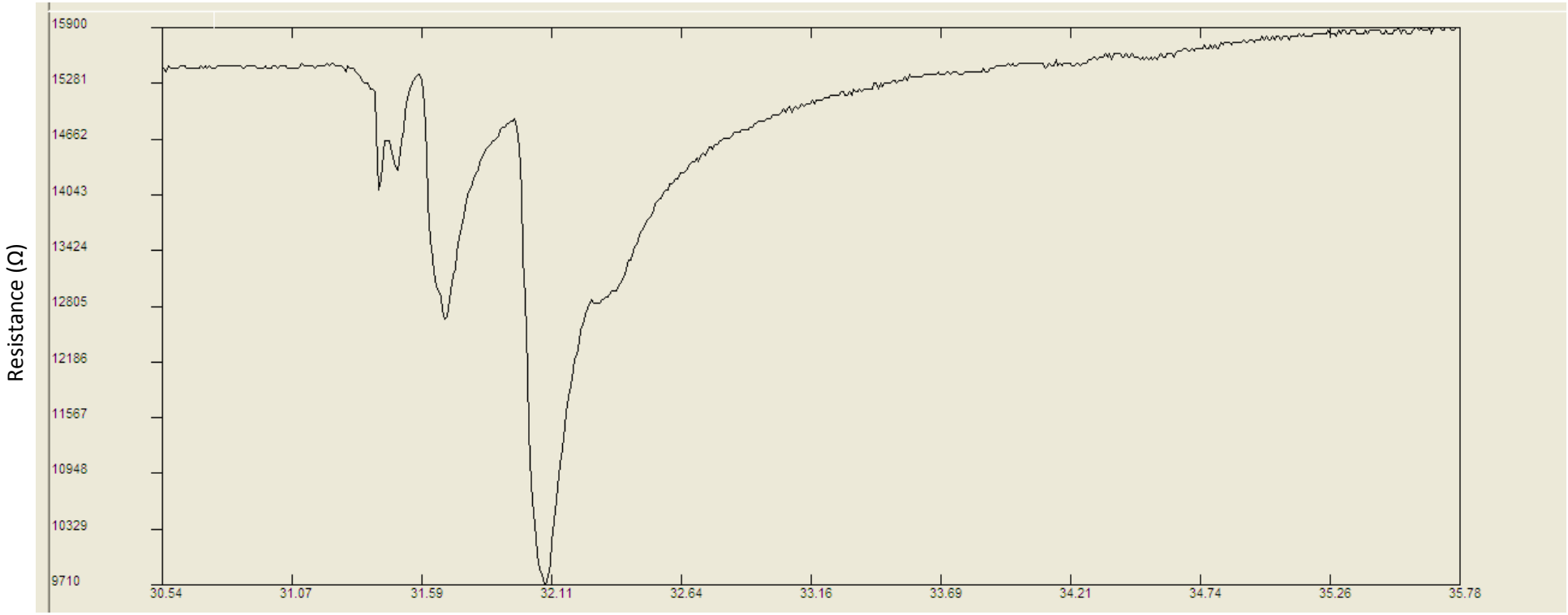

Figure 46 - Chromatogram showing the volatile trace pattern with time for *S. saprophyticus* $1.3x10^5$ Minutes 0-5 expanded

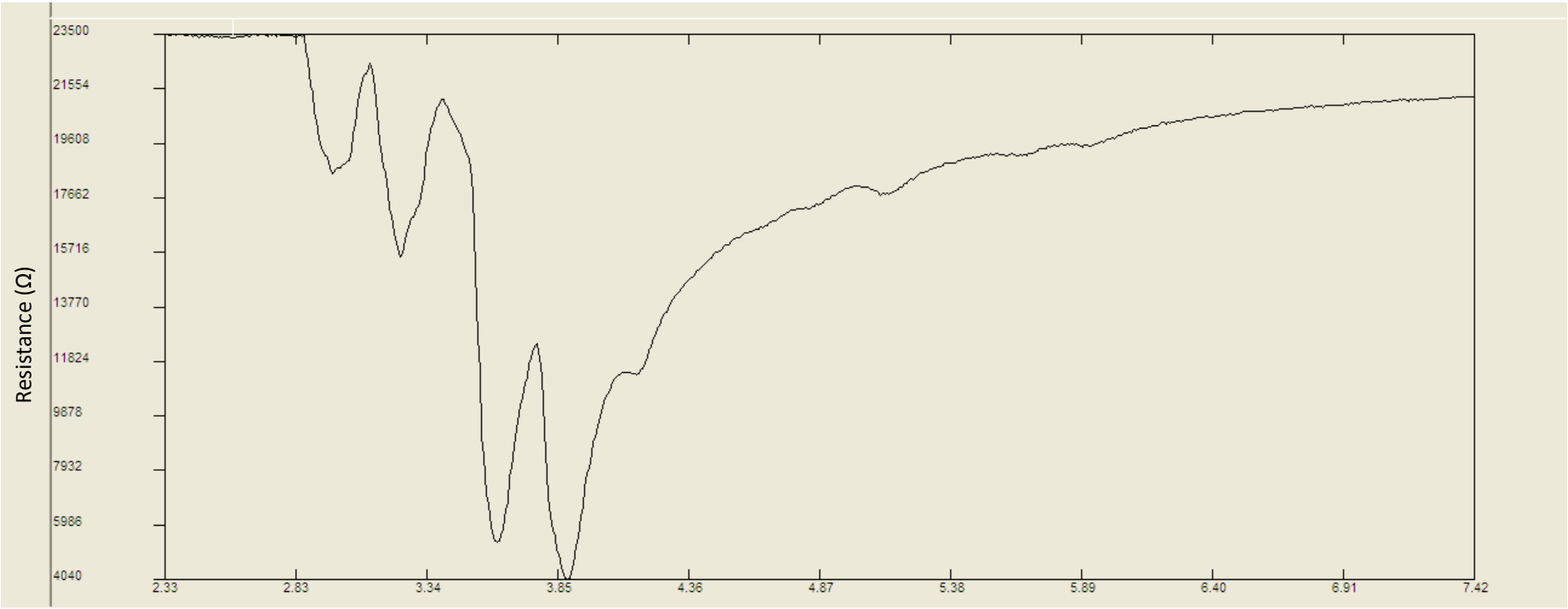

Figure 47 - Chromatogram showing the volatile trace pattern with time for *K. pneumoniae* $1.3x10^5$ Minutes 0-5 expanded

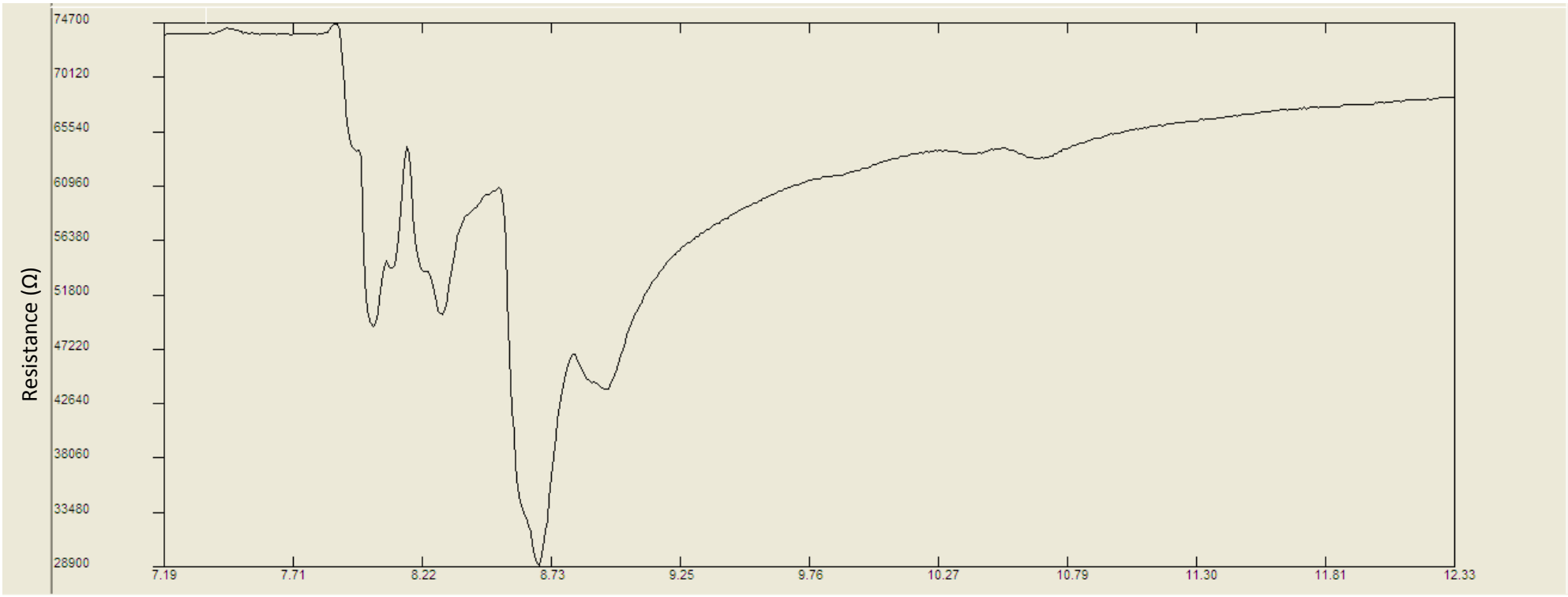

Figure 48 - Chromatogram showing the volatile trace pattern with time for *P. aeruginosa* $1.0x10^5$ Minutes 0-5 expanded

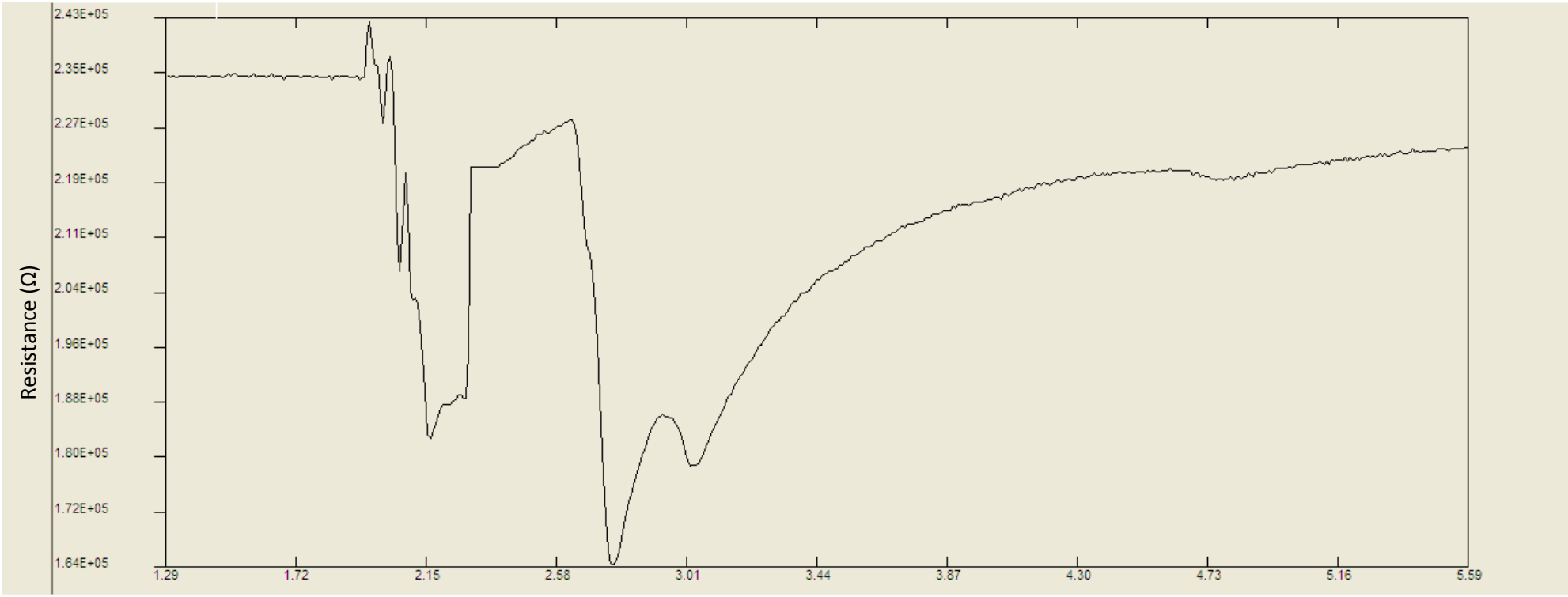

Figure 49 - Chromatogram showing the volatile trace pattern with time for *E. faecalis* $1.16x10^5$ Minutes 0-5 expanded

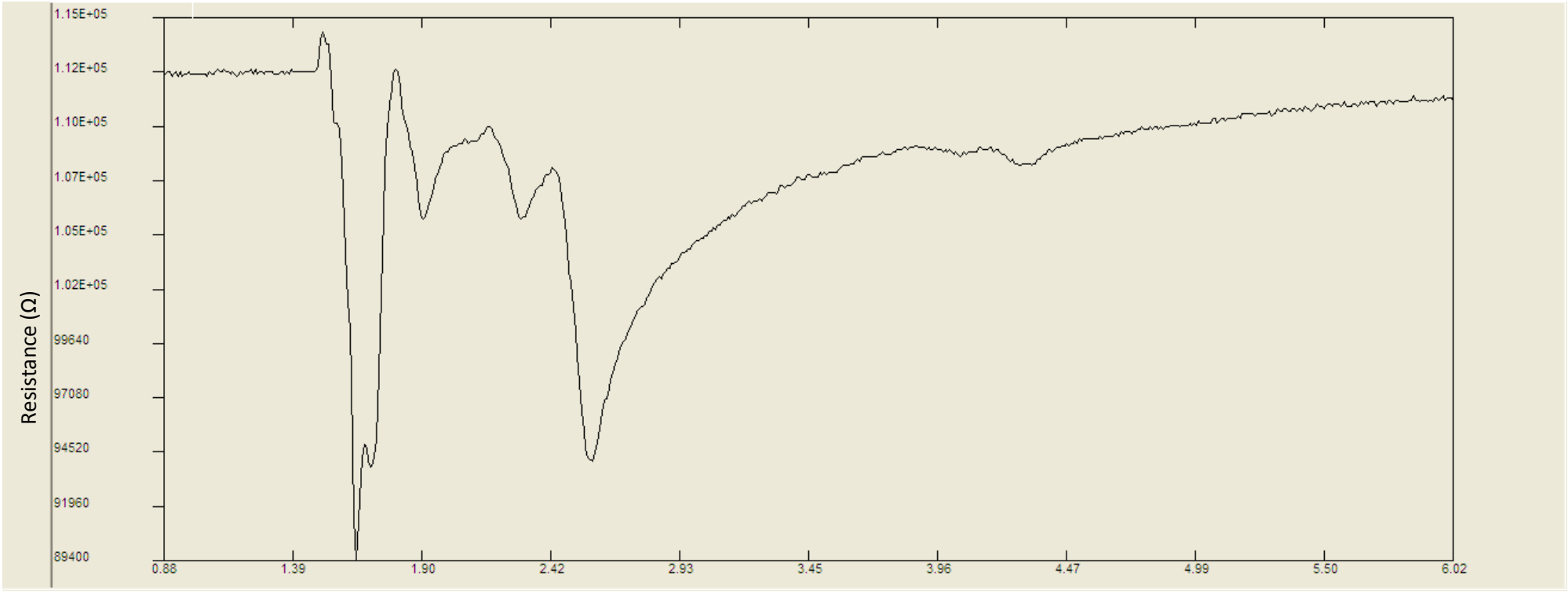

Figure 50 - Chromatogram showing the volatile trace pattern with time for *P. mirabilis* $1.2x10^5$ Minutes 0-5 expanded

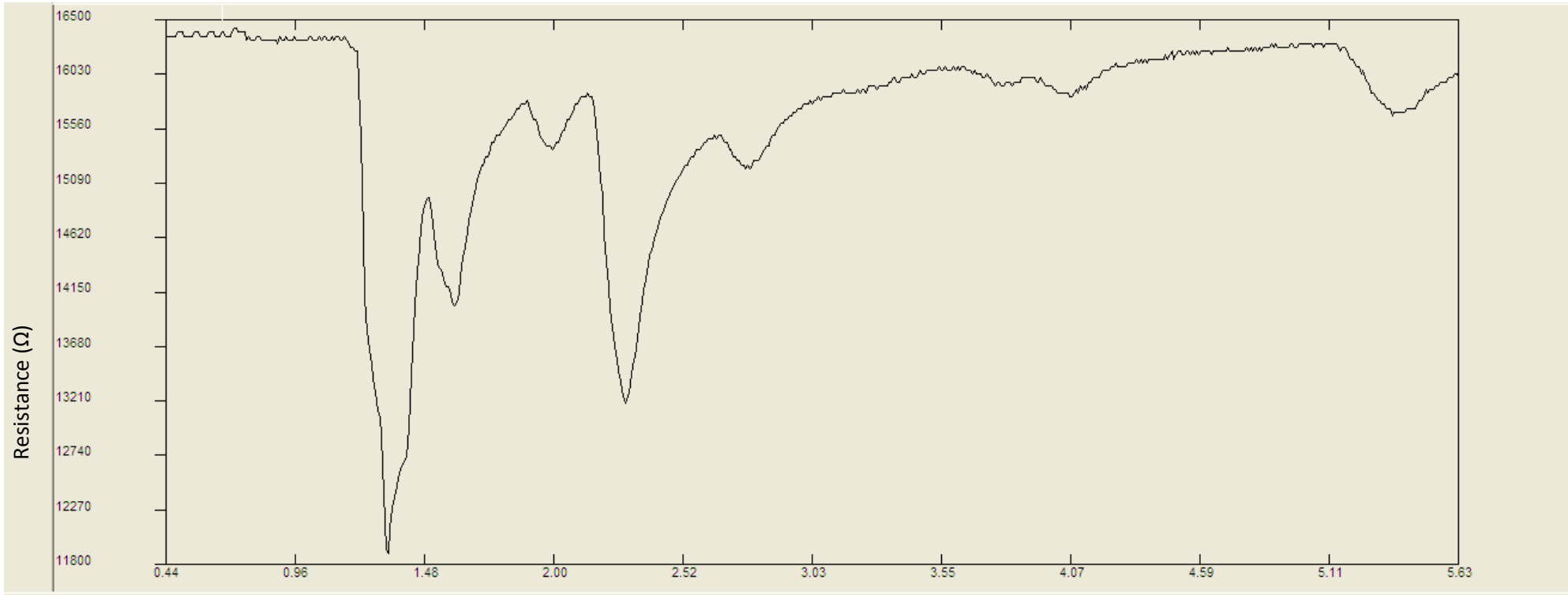

The first 5 minutes of each chromatogram has been expanded to show the volatile trace pattern for each bacteria. The number of significant peaks counted during this time is greater in some samples when compared to others e.g. *S. saprophyticus* contains 12 peaks whereas *P. mirabilis* contains 9. Even when the same number of significant peaks has been counted, e.g. *P .aeruginosa* and *P .mirabilis*, the volatile trace patterns are visibly different. A visual assessment of the chromatograms can assist in bacteria identification, however the retention time and percentage response of significant peaks must be known in order to accurately identify the UTI causing bacteria.

4.5.6 Identification of significant peak changes at retention time ranges

An analysis of the results was undertaken in order to identify significant peaks that underwent a change in height over the six hour test period. The retention time was used to identify each peak by way of determining how long it took for a particular volatile to pass through the system.

The percentage response and retention times of all significant peaks (3 x the size of the baseline) were obtained for each bacteria over the six hour test period. As a general rule, peaks less that 1.5% were disregarded, therefore any retention time range with a peak greater than 1.5% would be considered as an infected sample. Tables 29-33 show significant peak changes at retention time ranges for each of the 5 bacteria tested.

Table 29 *K. pneumoniae* - significant retention time ranges

K. pneumoniae

Hourly interval	Retention time range (minutes)			cfus/ml
	0.65-0.68	**0.86-0.89**	**9.93-9.99**	
Control	4.9%	0.0%	0.0%	0
Time0	23.4%	0.0%	1.5%	$1.6x10^4$
Time1	30.3%	9.6%	2.2%	$3.3x10^4$
Time2	30.3%	19.0%	2.4%	$1.3x10^5$
Time3	29.1%	4.5%	1.8%	$3.0x10^5$
Time4	29.8%	35.4%	3.3%	$5.3x10^5$
Time5	25.8%	34.8%	16.0%	$1.0x10^6$
Time6	28.6%	34.6%	30.9%	$3.3x10^7$

Between retention time range 0.65-0.68 a small peak is present in the control that is significantly higher at all other intervals. From time 1 onwards between retention time range 0.86-0.89, a peak appears that generally increases in height over the test period. During retention time range 9.93-9.99 a peak appears at time 0, slightly increasing in height until time5 where a significant height increase can be observed.

Table 30 *P. aeruginosa* - significant retention time ranges

P .aeruginosa

Hourly interval	Retention time ranges (minutes)			cfus/ml
	0.55-0.59	**0.63-0.67**	**1.58-1.59**	
Control	0.0%	4.9%	0.0%	0
Time0	-10.1%	20.9%	6.2%	$6.0x10^4$
Time1	-4.7%	13.6%	2.7%	$8.3x10^4$
Time2	6.5%	8.9%	4.1%	$1.0x10^5$
Time3	36.3%	33.1%	5.2%	$1.3x10^6$
Time4	11.1%	37.9%	5.2%	$3.3x10^6$
Time5	37.4%	33.7%	12.8%	$3.6x10^6$
Time6	46.1%	40.5%	26.6%	$5.6x10^6$

During retention time 0.55-0.59 an upward peak appears at time 0 that generally increases in height throughout the test period, the same can be said for retention time 1.58-1.59. A small peak is present in the control during retention time 0.63-0.67 that generally increases in height throughout the test period.

Table 31 *E. faecalis* - significant retention time ranges

E. faecalis

Hourly interval	Retention time ranges (minutes)			cfus/ml
	0.64-0.65	**1.30 -1.42**	**1.59-1.66**	
Control	0.0%	53.1%	0.0%	0
Time 0	19.2%	1.90%	8.14%	$5.6x10^4$
Time1	23.1%	4.10%	14.73%	$1.16x10^5$
Time2	25.1%	5.70%	20.10%	$3.6x10^5$
Time4	0.0%	6.30%	1.50%	$1.3x10^7$
Time5	25.9%	3.50%	13.88%	$1.0x10^5$
Time6	30.7%	5.60%	15.70%	$1.3x10^5$

During retention time ranges 0.64-0.65 and 1.59-1.66, a peak appears at time 0 that generally increases in height throughout the test period, however time 4 does not follow this trend. During retention time range 1.30-1.42 a large peak can be observed in the control that is much smaller at all other hourly intervals.

Table 32 *P. mirabilis* - significant retention time ranges

P. mirabalis

Hourly interval	Retention time ranges (minutes)		cfus/ml
	0.59-0.64	**0.87-0.89**	
Control	0.0%	0.0%	0
Time0	6.5%	0.0%	$1.3x10^4$
Time1	11.9%	7.4%	$1.6x10^4$
Time2	25.3%	4.5%	$2.3x10^4$
Time3	17.7%	5.8%	$1.2x10^5$
Time4	41.2%	0.0%	$2.3x10^5$
Time5	52.6%	29.8%	$4.3x10^5$

A peak appears at time 0 during retention time range 0.59-0.64, generally increasing in height at each interval. During retention time range 0.66-0.68 the peak present generally increases in height until time 4 where the peak decreases in height until time 5. Time 6 has been discounted due to an error when the sample was injected. A peak appears at time 1 during retention time range 0.87-0.89 that generally increases in height at each hourly interval. Time 4 is an anomalous result that does not follow this trend.

Table 33 *S. saprophyticus* - significant retention time ranges

S. saprophyticus

Hourly interval	Retention time ranges (minutes			cfus/ml
	1.26-1.28	**1.3-1.36**	**5.34-5.45**	
Control	0.0%	53.1%	0.0%	0
Time1	0.0%	8.1%	5.9%	$1.6x10^4$
Time2	504.8%	35.5%	12.3%	$1.0x10^4$
Time3	322.0%	34.9%	9.4%	$3.3x10^4$
Time4	126.1%	12.8%	24.1%	$1.3x10^5$
Time5	261.7%	420.7%	37.8%	$3.3x10^5$
Time6	0.0%	472.6%	26.3%	$1.3x10^5$

During retention range 1.23-1.28 a large peak appears at time 2 that generally decreases in height until time 6 where the peak is no longer present. A peak present in the control during retention time range 1.3-1.36 generally decreases in height until time 5, where a significant increase can be observed. A peak appears at time 1 during retention time range 5.34-5.45 that generally increases in height at each hourly interval. Time 0 has been discounted due to error when injecting the sample.

4.5.7 Summary

The data from the above section was collated into one table (table 34).

Table 34 - Significant changes at retention times for 5 common UTI causing bacteria

Bacteria	**Retention time range 1**	**Retention time range 2**	**Retention time range 3**
K .pneumoniae	0.65-0.68[a]	0.86-0.89≥time1	9.93-9.99≥time0
P. aeruginosa	0.55-0.59≥time2	0.63-0.67[a]	1.58-1.59≥time0
E. faecalis	0.64-0.65≥time0	1.30 -1.42[b]	1.59-1.66≥time0
P. mirabilis	0.59-0.64≥time0	0.87-0.89≥time1[c]	
S. saprophyticus	1.26-1.28≥time2	1.3-1.36≥time5	5.34-5.45≥time1

[a] Small peak in control, much higher at all other intervals
[b] Large peak in control that is smaller at all other intervals
[c] Anomalous result for time4

Table 34 shows retention time ranges indicating bacterial growth for all 5 bacteria. This not only shows that bacteria can be detected using this method, but also that the causing bacteria can be tentatively identified using the unique retention time ranges. Occasionally there is an overlap in retention time ranges between bacteria e.g. 1.30-1.42 *E. faecalis* and 1.3-1.36 *S. saprophyticus*, however when used in combination with retention time ranges 1 and 3, differentiation is possible.

Using these retention time ranges bacteria can be detected in less than 10 minutes. Microbial testing can take up to 6 days, making these tests much faster.

4.6 Alkaline samples

It is well known that bacteria can produce amines and ammonia. In slightly acidic urine, these will have low volatility because the ammonia and amines are protonated and therefore effectively in-volatile. The addition of alkaline reduces the acidity and thereby frees the amines and ammonia which can then form part of the headspace.

To test this, the method described above was used to inoculate filtered human urine with three different strains of bacteria. These bacteria were *E. faecalis*, *P. aeruginosa* and *S. epidermidis*. In these tests the samples were made alkaline. Volatile analysis of the inoculated urine was assessed at hourly intervals over a 4 hour period, the first sample being taken at time zero. A bacteria count and optical density measurement was also undertaken at the same time as the volatile analysis.

A control of filtered urine with no added bacteria was run on the same day as each bacteria, serving as a comparison between the volatile traces of an uninfected urine and inoculated urine.

At each hourly interval, 1.5ml of sodium hydroxide (1Mol) was added to 1.5ml of inoculated urine (and uninfected urine for the control) in a headspace sampling vial. The vial was placed into a water bath at 60°C for 10 minutes. The vial was then removed and $2cm^3$ of the headspace gases were extracted using a hypodermic needle and a glass syringe. The headspace gases were then injected into the GC column. The initial GC oven temperature was 40^oC with a 6 minute hold at this temperature, then the temperature was ramped up at a rate of 5^oC/min to 100^oC with a 22 minute hold at this temperature to give a total run time of 42 minutes. The carrier gas

(air) pressure was 35 psi. To ensure that the glass syringe did not absorb any volatiles from the previous sample, it was placed in an oven for 60 minutes at 200°C between each use.

4.6.1 A visual assessment of chromatogram results

A chromatogram was generated by GCDetector ANN/OdoReader for each hourly interval with all 3 bacteria. Figure 51 shows a screen shot of the control which was used to compare samples infected with known bacteria. Figures 52- 54 show representative screen shots of the chromatograms for all 3 bacteria at roughly 10^6 cfus/ml, during the first five minutes of the 42 minute run. It was found that nearly all significant peak changes happened in during the first five minutes.

Figure 51 – Chromatogram showing the volatile trace pattern with time for the control Minutes 0-5 expanded

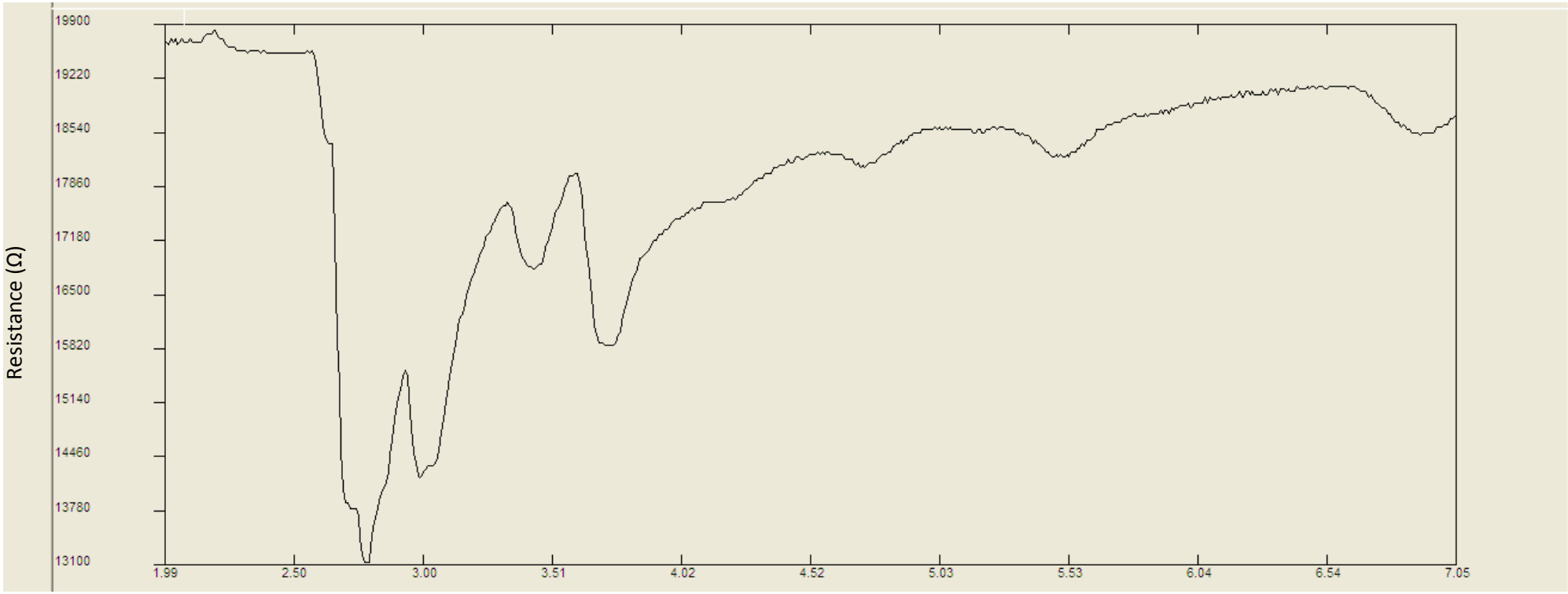

Figure 52 - Chromatogram showing the volatile trace pattern with time for *S. epidermidis* 3.40 x10^6 Minutes 0-5 expanded

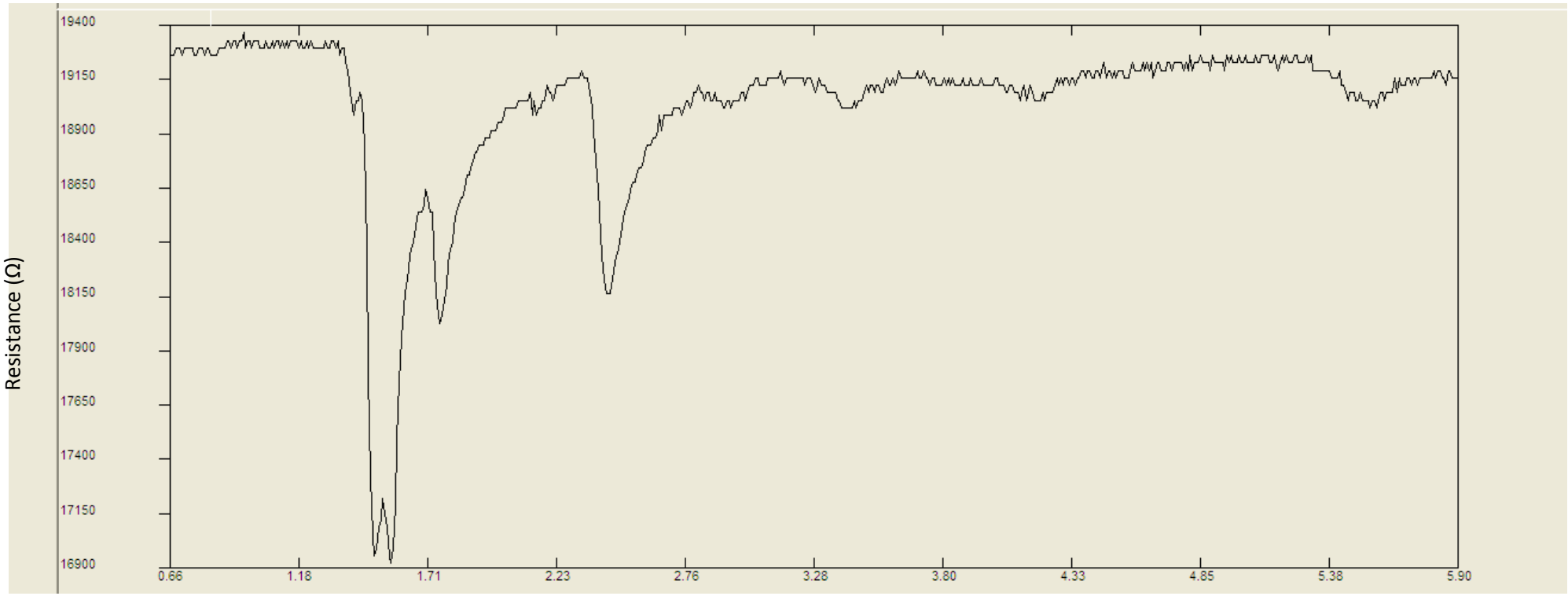

Figure 53 - Chromatogram showing the volatile trace pattern with time for *E .faecalis* 4.33x10^6 Minutes 0-5 expanded

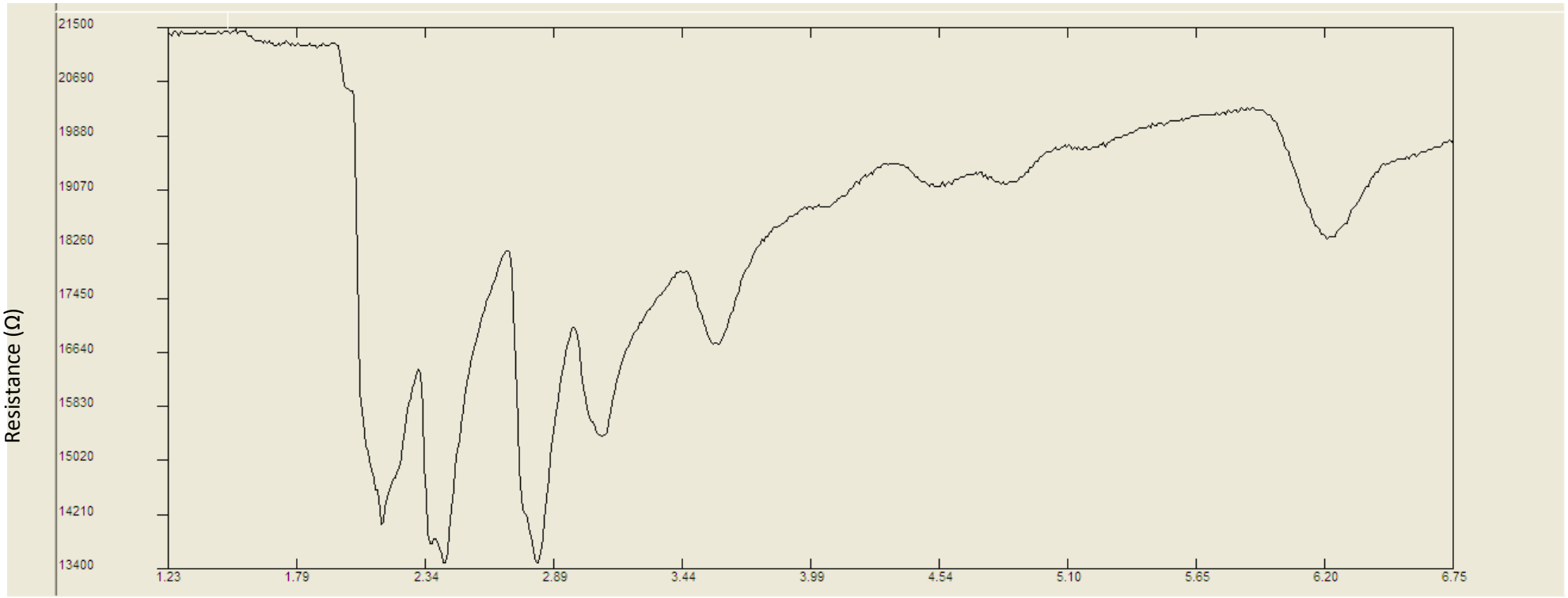

Figure 54 - Chromatogram showing the volatile trace pattern for *P. aeruginosa* 5.33 x10^6. Minutes 0-5 expanded

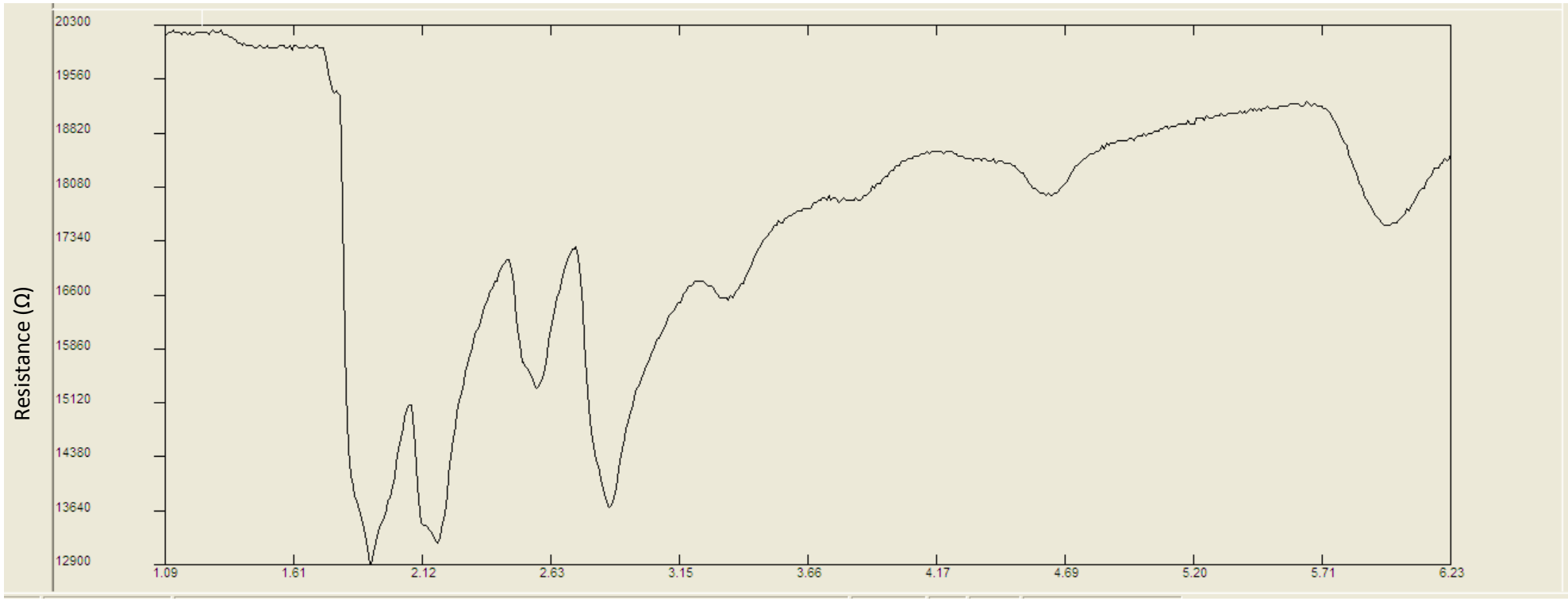

Screen shots taken of each bacteria at roughly the same concentration shows visible difference between the volatile trace patterns of each bacteria. These differences are even more apparent once the first 5 minutes have been expanded. Very few peaks can be observed in the sample containing the *S. epidermidis* bacteria at this concentration compared to *P. aeruginosa* and *E. faecalis.* Although *P. aeruginosa* and *E. faecalis* samples contain a similar number of peaks, the trace patterns are not the same, which shows promise in the ability to differentiate between different UTI causing bacteria.

4.6.2 Identification of significant peak changes within certain retention time ranges

The retention times and percentage responses for all significant peaks (3 x the size of the baseline) were collected for each bacteria over the four hour test period. Retention time ranges that underwent a change in peak size as the bacterial count went up were identified. These retention time ranges can be seen in tables 35-37.

Table 35 *E .faecalis* - significant retention time ranges

E. faecalis

Hourly interval	Retention time range (minutes)			cfus/ml
	0.87-0.9	**1.27-1.31**	**1.52-1.61**	
Control	37.7%	77.2%	1.7%	0
Time0	19.1%	27.0%	10.6%	$4.33x10^6$
Time1	7.2%	1.8%	16.7%	$1.00x10^7$
Time2	4.8%	1.8%	10.6%	$1.60\ x10^7$
Time3	7.9%	1.9%	16.9%	$2.67\ x10^7$
Time4	8.4%	1.9%	20.2%	$5.33\ x10^7$

During retention time range 0.87-0.9 and 1.27 – 1.31 there is a large peak present at time 0 that is significantly smaller as bacteria grows and time progresses. The change in peak height between retention time range 1.52-1.61 is too variable for diagnostic use, however it has been included here as the peak height has increased significantly when compared to the control.

Table 36 *S. epidermidis* - significant retention time ranges

S. epidermidis

Hourly interval	Retention time range (minutes)			cfus/ml
	1.59-1.63	**19.54-19.63**	**26.2-26.75**	
Control	0.0%	0.0%	0.0%	0
Time0	19.7%	0.0%	3.5%	6.67×10^5
Time1	3.4%	2.8%	1.3%	1.03×10^6
Time2	12.9%	6.1%	2.8%	1.40×10^6
Time3	5.5%	1.5%	1.0%	2.60×10^6
Time4	25.9%	10.0%	3.1%	3.40×10^6

There is no peak present in the control during retention time range 1.59-1.63 however one does appear from time 0 onwards. This peak varies in height over the 4 hour test period so its presence alone could not be used to identify bacterial concentration. During retention time range 19.54-19.63 a peak appears from time 1 onwards varying in height over the 4 hour test period. Significant peak changes can be observed much later on for samples inoculated with this bacteria i.e. during retention time ranges 19.54-19.63 and 26.2-26.75. This is most likely due to much larger volatiles in the sample taking longer to elute from the column.

Table 37 *P. aeruginosa* - significant retention time ranges

P. aeruginosa

Hourly interval	Retention time range (minutes)			cfus/ml
	0.88-0.9	**1.33**	**4.68-4.83**	
Control	0.00%	0.00%	0.00%	0
Time0	0.00%	59.00%	5.80%	8.33×10^5
Time1	0.00%	28.90%	11.20%	6.67×10^5
Time2	12.40%	2.20%	9.70%	1.27×10^6
Time3	1.90%	2.80%	1.10%	5.33×10^6
Time4	15.40%	15.80%	8.90%	2.00×10^7

A peak appears at time 2 between retention time range 0.88-0.9, however an anomalous result can be observed at time 3. At retention time 1.33 there is a large peak present at time 0 (that is not in the control) that is smaller at all other samples as time progresses. During retention time range 4.68-4.83 there is no peak in the control, however one does appear from time 0 onwards. This peak varies in height over the 4 hour test period so its presence alone could not be used to identify bacterial concentration.

4.6.3 Summary

The data from the above section was collated into one table (table 38).

Table 38 Significant changes at retention times for 3 common UTI causing bacteria treated with alkaline

S. epidermidis	1.59-1.63≥time0	19.54 19.63≥time1	26.2-26.75≥time0
P. aeruginosa	0.88-0.9≥time2	1.33≥time0[b]	4.68-4.78≥time0
E. faecalis	0.87-0.90[a]	1.27-1.31[a]	1.52-1.61[b]

[a] Peaks generally getting smaller in height
[b] Small peak in control that increases in height over the test period

The table shows that using the unique retention time ranges bacteria in human urine can be detected. Differentiation between each bacteria is also possible using these ranges, even when there is an overlap i.e. for *E. faecalis*, 0.87-0.9 and *P. aeruginosa* 0.88-0.9, as the peaks behave differently, generally decreasing in height for *E. faecalis* and increasing in height for *P.aeruginosa.*

4.7 Comparison between alkaline and non alkaline controls

An inspection of the chromatogram of the non alkaline control showed that there were 16 peaks as opposed to 39 peaks in the control with alkaline added (see figure 55). The much larger number of peaks in the alkaline control must be due to chemical reactions producing many more VOCs. This is consistent with previous work by Steve Smith (UWE) using a different analytical technique (GC/MS). It might be expected that the greater number of compounds would potentially enhance the discrimination between bacteria in chemically treated urine.

Figure 55 Graph showing retention times and percentage responses for non alkaline control and alkaline control

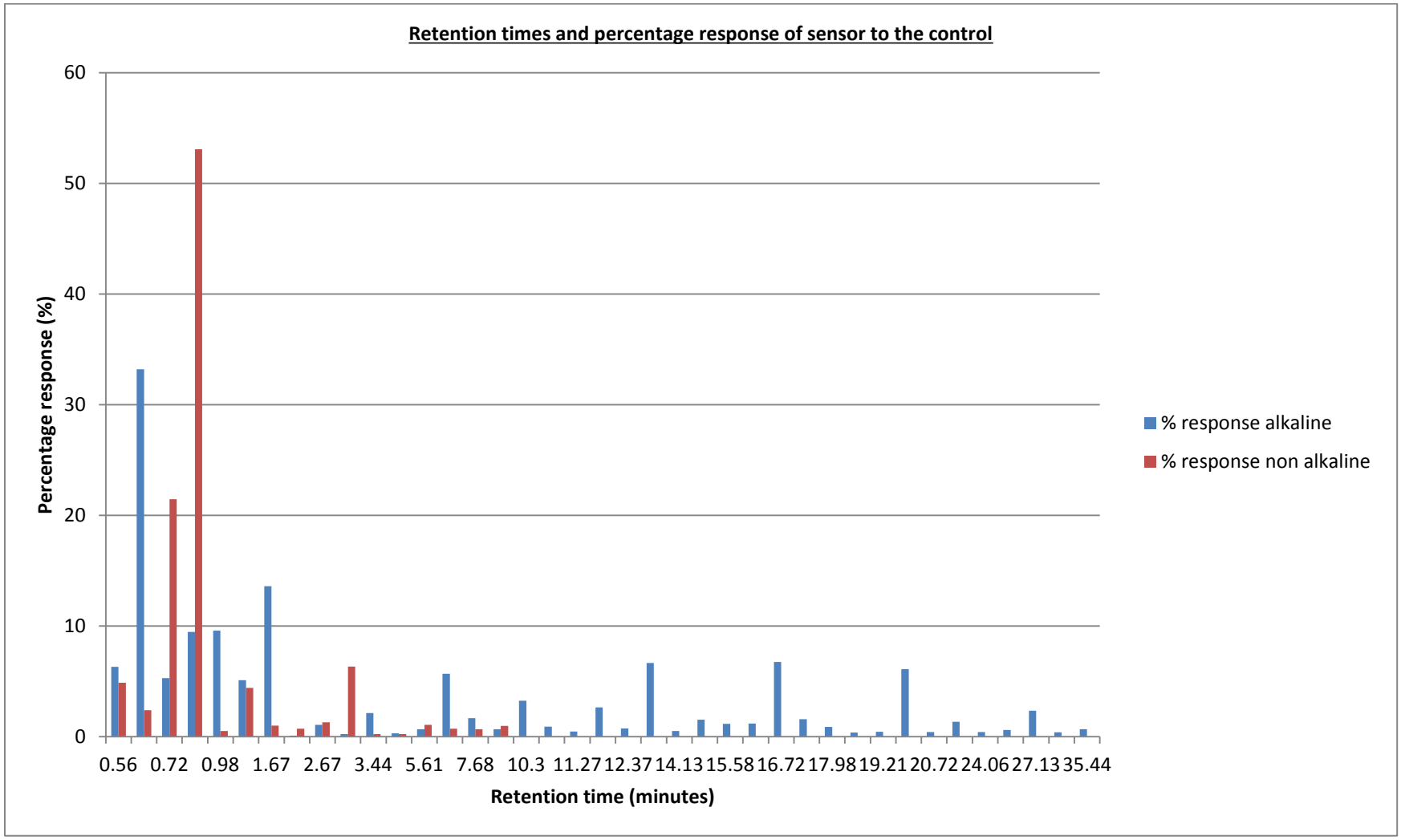

4.7.1 Comparison between alkaline and non alkaline samples infected with the same bacteria

Bacteria added to urine made alkaline and non alkaline are compared here. The same number of significant retention time ranges can be observed for alkaline and non alkaline samples. Different retention time ranges can also be observed for alkaline and non alkaline samples inoculated with the same bacteria (see table 39). Even when these retention time ranges overlap slightly i.e. non alkaline *E. faecalis* during retention time range 1.30-1.42 and alkaline *E .faecalis* 1.27-1.31 alkaline, the significant peaks behave differently generally increasing in height in non alkaline samples and decreasing in height in alkaline samples. Further work needs to be undertaken to ascertain whether alkaline treated samples or un-treated samples are better for differentiating between bacterial species.

Table 39 Comparison between significant peak changes for alkaline samples and non alkaline

Bacteria	**Retention time range 1**	**Retention time range 2**	**Retention time range 3**
P. aeruginosa **non** alkaline	0.55-0.59≥time2	0.63-0.67[a]	1.58-1.59≥time0
P. aeruginosa alkaline	0.88-0.9≥time2	1.33≥time0[c]	4.68-4.78≥time0
E. faecalis **non** alkaline	0.64-0.65≥time0	1.30-1.42[a]	1.59-1.66≥time0
E. faecalis alkaline	0.87-0.9[c]	1.27-1.31[c]	1.52-1.61[a]

[a] Small peak in control, increases in height over the test period
[b] Large peak in control that is smaller at all other intervals
[c] Peaks getting smaller in height

4.8 Conclusion

Using OdoReader the detection of bacteria in human urine (at UTI levels) has been possible by looking at the retention times and percentage responses of significant peaks.

The results show that there is the potential to differentiate between bacteria by looking for the presence of peaks at retention time ranges. Further work needs to undertaken in order to establish the reproducibility of these results and upon the success of this, an extensive study using samples from patients known/suspected of having a UTI.

If this further work is successful the low production cost of OdoReader would make it an attractive diagnostic device for point of care use in general practice, surgeries and hospitals.

4.9 Overall summary

A new mini gas sensor for medical diagnostic applications has been developed here. Results show that this sensor is highly reproducible especially in regards to the resistance of the heater element (of 25 sensors tested, a mean of 10.8Ω at 0°C, S.D. 0.23Ω). The sensor also met sensitivity requirements outlined at the start of the project and a mean (of 25 sensors) sensitivity of 216%, S.D. 46% was recorded in response to 50ppm ethanol injections.

Sensors have been installed in 3 OdoReader systems at Bristol Royal Infirmary and run continuously for over six months with no reported failures i.e. heaters burning out/ loss of electrical connection. This sensor has a lifespan that is considerably longer compared to sensors previously bought commercially for similar work. It has been reported that sensors have responded well to biological samples (stool) and ethanol standards over this six month period.

A pilot study was undertaken to assess the potential for bacterial identification and urinary tract infection (UTI) diagnosis through volatile organic compound (VOC) analysis. The sensor was used in combination with a GC column (OdoReader) to assess urine inoculated with known bacteria.

Using the OdoReader system and GC detection software *(*GCDetector ANN), unique retention time ranges were identified for the bacteria tested. The results showed that the presence of bacteria in human urine could be detected (in less than 10 minutes) and that there is also the potential for identification of the UTI causing bacteria. This pilot study has shown that VOC analysis is a promising methodology that would merit a more extensive study.

Chapter 4 References

45.Khatun S. Mahmood A. Nessa A. (1999) Urinary Tract Infections in Pregnancy, The ORION. Vol. 4

46. Al Singary W. Elder JB. Holland TA. Spanel P. Smith D. (1999) Analysis of Formaldehyde in the headspace of urine from bladder and prostate cancer patients using selected ion flow tube mass spectroscopy, Commun.Mass Spectrom. Vol. 13, Issue 14 Pgs 1354-1359

47. Mills GA. Walker V. (2001) Headspace solid-phase microextraction profiling of volatile compounds in urine: application to metabolic investigations. J. Chromatogr. B: Biomed. Sci, Appl. Vol. 753, Issue 2 Pgs 259-268

48. Avesh R. Mitchell SC. Smith RL. Zhang AQ (1992) Determination of trimethylamine and related aliphatic amines in human urine by head-space gas chromatography, J. Chromatogr : Biomed. Appl. Vol. 584, Issue 2, Pgs 141-145.

49. Barnsbury AJ. Church JCT. Church SM. Cook AW. Willis CM. (2004) Olfactory detection of human bladder cancer by dogs: proof of principle study. BMJ. Vol. 329, Pgs 329-712